A General Approach to Lifting-Line Theory, Applied to Wings with Sweep

Jackson T. Reid* and Douglas F. Hunsaker†
Utah State University, Logan, Utah, 84321, USA

Implementations of lifting-line theory model the flow over a finite wing using a sheet of semi-infinite vortices extending from a vortex filament placed along the locus of aerodynamic centers of the wing. Prandtl's classical implementation is restricted to straight wings in flows without sideslip. In this work, it is shown that these limitations can be overcome if, at the control points where induced velocity is calculated, the second derivative of the locus of aerodynamic centers is zero and the trailing vortices are perpendicular to the locus. Therefore, a general implementation of lifting-line theory is presented that conditionally forces the second derivative of the locus of aerodynamic centers to zero at each control point, and joints each trailing vortex such that there is a finite segment of the trailing vortex perpendicular to the locus of aerodynamic centers. Consideration is given to modeling the locus of aerodynamic centers of non-straight wings and the section aerodynamic properties of such wings. The resulting general formulation is analyzed to determine sensitivity, accuracy, and numerical convergence. The general implementation demonstrates second-order convergence when the control points are clustered at the root and tips of the wing, and produces results that closely match those of a higher-order panel method and experimental data.

I. Introduction

Lifting-line theory is based on the conjecture made in the study of potential flow that the physical flow around a body can be represented as the velocity field induced by a distribution of vortices added to a freestream [1–4]. In particular, lifting-line theory asserts that the flow over a finite, high-aspect-ratio wing is sufficiently represented by a sheet of semi-infinite vortices extending from a single, variable strength vortex filament, placed along the locus of aerodynamic centers of the wing, as depicted in Fig. 1. To satisfy Helmholtz's vortex laws, the circulation distribution of the vortex sheet is defined as the change in the circulation distribution of the bound vortex filament. The crux of lifting-line theory is the determination of the circulation distribution that results in a field of induced velocity along the bound vortex filament that is sufficiently representative of velocity experienced by the corresponding physical wing, for a given freestream condition.

In Prandtl's classical derivation of lifting-line theory [1], the circulation distribution, $\Gamma(z)$, is found by equating two definitions for the section lift coefficient, $\tilde{C}_L$. First, from the Kutta-Joukowski law, the section coefficient of lift is given by

$$\tilde{C}_L = \frac{2\Gamma}{V_\infty c} \tag{1}$$

Second, it is assumed that the section lift coefficient is a linear function of angle of attack

$$\tilde{C}_L = \tilde{C}_{L,\alpha}(\alpha_{\text{eff}} - \alpha_{L0}) \tag{2}$$

where $\tilde{C}_{L,\alpha}$ and α_{L0} are properties of the section airfoil, and α_{eff} is the effective angle of attack. The effective angle of attack deviates from the global angle of attack of the wing, α, due to the velocity that the semi-infinite vortex sheet induces along the locus of aerodynamic centers. Assuming that the velocity induced by the vortex sheet is small compared to the freestream, the effective angle of attack is

$$\alpha_{\text{eff}}(z_0) = \alpha - \frac{1}{4\pi V_\infty}\int_{-b/2}^{b/2} \frac{(d\Gamma/dz)}{z_0 - z} dz \tag{3}$$

*PhD Candidate, Mechanical & Aerospace Engineering, 4130 Old Main Hill, AIAA Student Member.
†Assistant Professor, Mechanical & Aerospace Engineering, 4130 Old Main Hill, AIAA Member.

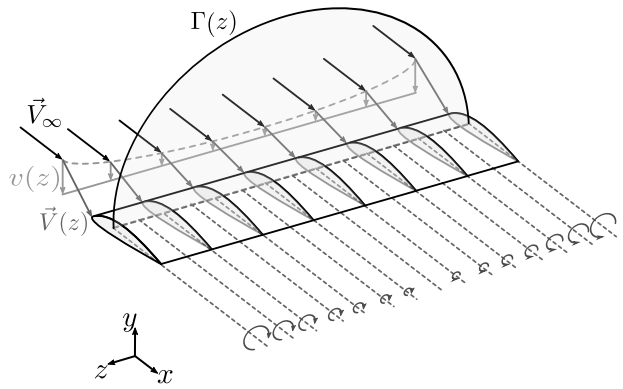

Fig. 1 Depiction of Prandtl's classical lifting-line theory.

where z_0 is a spanwise location along the wing, see Fig. 1. In the case of a wing without sweep or dihedral, the locus of aerodynamic centers is assumed to lie along a straight line. Hence, the bound vortex filament does not have any effect on the effective angle of attack. Equating Eqs. (1) and (2), in combination with Eq. (3) results in Prandtl's fundamental lifting-line theory equation for a given section, z_0, along the wing

$$\alpha(z_0) = \frac{2\Gamma(z_0)}{V_\infty c(z_0) C_{\tilde{L},\alpha}(z_0)} + \alpha_{\tilde{L}=0}(z_0) + \frac{1}{4\pi V_\infty} \int_{-b/2}^{b/2} \frac{(d\Gamma/dz)}{z_0 - z} dz \tag{4}$$

where the only unknown is the circulation distribution, $\Gamma(z)$.

In order to find a lift distribution that satisfies Eq. (4), consider the change of variables

$$z = -\frac{b}{2}\cos(\theta) \tag{5}$$

$$dz = \frac{b}{2}\sin(\theta) d\theta \tag{6}$$

With this transformation of variables, the general circulation distribution, $\Gamma(z)$, can be expressed as the Fourier sine series

$$\Gamma(\theta) = 2bV_\infty \sum_1^\infty A_n \sin(n\theta) \tag{7}$$

whose derivative is

$$\Gamma'(z) = \frac{d\Gamma}{dz} = \frac{d\Gamma}{d\theta}\frac{d\theta}{dz} = 2bV_\infty \sum_1^\infty n A_n \cos(n\theta)\frac{d\theta}{dz} \tag{8}$$

The required Fourier coefficients, A_n, are found by evaluating Eq. (4) at N sections along the wing. The solution to the resulting system of equations provides the first N coefficients of the circulation distribution, $\Gamma(\theta)$. Thus, Eq. (4) can be rewritten as

$$\begin{aligned} \alpha(\theta_0) &= \frac{4b}{c(\theta_0) C_{\tilde{L},\alpha}(\theta_0)} \sum_1^N A_n \sin(n\theta_0) + \alpha_{\tilde{L}=0}(\theta_0) + \frac{1}{\pi}\int_0^\pi \frac{\sum_1^N n A_n \cos(n\theta_0)}{\cos(\theta) - \cos(\theta_0)} d\theta \\ &= \frac{4b}{c(\theta_0) C_{\tilde{L},\alpha}(\theta_0)} \sum_1^N A_n \sin(n\theta_0) + \alpha_{\tilde{L}=0}(\theta_0) + \sum_1^N n A_n \frac{\sin(n\theta_0)}{\sin(\theta_0)} \end{aligned} \tag{9}$$

for each of the N sections along the wing.

While this classical version of lifting-line theory is applicable to, and provides valuable intuition into, the aerodynamic behavior of straight, high aspect ratio, finite wings in flows without sideslip, it is unusable for any other category of wing.

Previous attempts have been made to extend lifting-line theory to wings with sweep. One commonly used method moves the control points off the locus of aerodynamic centers to the three-quarter chord line [5–7]. This method then constrains the total velocity at each control point to be tangential to the wing camber line. The downside of this approach is that it is no longer possible to use arbitrary section properties that account for thickness or contain viscous corrections to the lift slope. Another method is to apply a finite core, or another type of integral cutoff, to the vortex models [8–10]. However, these cutoff methods can be very sensitive to the cutoff/core distance, and thus require precise tuning of the method, making it dependent on known data. Furthermore, a numerical adaptation of Prandtl's lifting-line implementation was developed by Phillips [11]. However, that algorithm suffers from an inability to numerically grid-converge for for wings with sweep or in sideslip—as will be shown hereafter. Nevertheless, the advantage of Phillips' method lies in the fact that explicit integration is not necessary in the determination of induced velocity, as opposed to Eq. (3). This advantage is leveraged in the derivation of a general implementation of lifting-line theory.

The work herein is focused on a generalized implementation of lifting-line theory, allowing for its application to wings with sweep and wings in sideslip. Although work has been performed on the topic of low aspect-ratio wings [2, 12, 13], it will not be addressed in this work. It is desirable to obtain a method with which the aerodynamic properties of swept wings can be predicted, while avoiding the drawbacks of other proposed methods. The general implementation of lifting-line theory derived in this work maintains the ability to use an arbitrary model of section properties, remains relatively insensitive to model tuning parameters, and grid resolves.

II. Induced Velocity

The first step in deriving a general implementation of lifting-line theory is to describe the velocity induced along the locus of aerodynamic centers more generally than the description in Eq. (3). The velocity induced at each point along the wing is found by considering the influence of the trailing vortex sheet and the bound vortex filament, for a locus of aerodynamic centers described by the general function, $f(z)$, in the $x - z$ plane.

A. Influence of the Bound Vortex Filament

The velocity induced by a differential element of the vortex filament at a point along the locus of aerodynamic centers, $\vec{x}_0 = [f(z_0), 0, z_0]$, is governed by the Biot-Savart law [3]

$$d\vec{V} = \frac{\Gamma}{4\pi}\frac{d\vec{l}\times\vec{r}}{r^3} \tag{10}$$

where the vectors $d\vec{l}$ and $\vec{r}$ are defined as

$$d\vec{l} = -\frac{d}{dz}\Big[f(z), 0, z\Big] = -\Big[f'(z), 0, 1\Big]dz \tag{11}$$

$$\vec{r} = \Big[f(z_0) - f(z), 0, z_0 - z\Big] \tag{12}$$

and r is the magnitude of $\vec{r}$. Thus, the influence of a differential element of the vortex filament placed on the locus of aerodynamic centers can be described as

$$d\vec{V}_{\mathrm{LAC}}(z_0) = \frac{-\Gamma(z)}{4\pi}\frac{\left[0, \frac{f(z_0)-f(z)}{z_0-z} - f'(z), 0\right]}{\left(1 + \left(\frac{f(z_0)-f(z)}{z_0-z}\right)^2\right)^{3/2}(z_0 - z)^2}dz \tag{13}$$

The total velocity induced at the point z_0 by the entire bound vortex filament is found through the integration of Eq. (13)

$$\vec{V}_{\mathrm{LAC}}(z_0) = \int_{-b/2}^{b/2}\frac{-\Gamma(z)}{4\pi}\frac{\left[0, \frac{f(z_0)-f(z)}{z_0-z} - f'(z), 0\right]}{\left(1 + \left(\frac{f(z_0)-f(z)}{z_0-z}\right)^2\right)^{3/2}(z_0 - z)^2}dz \tag{14}$$

1. Conditions on Bound Vortex Filament

It is seen that the integral in Eq. (14) contains singularities at $z = z_0$. The limit at that point is found to be

$$\lim_{z\to z_0} d\vec{V}_{\mathrm{LAC}}(z_0) = \frac{-\Gamma(z_0)}{4\pi}\frac{\left[0, f''(z_0), 0\right]}{3\Big(1 + f'(z_0)^2\Big)^{3/2}(z_0 - z_0)}dz \tag{15}$$

Because of the second term in the denominator, this limit is infinite unless $f''(z_0)$ or $\Gamma(z_0)$ is zero, in which case the limit becomes indeterminate. To be useful in lifting-line theory, $\Gamma(z_0)$ must be allowed to remain non-zero. Accordingly, consider the case that

$$f''(z_0) = 0 \tag{16}$$

The limit at z_0 can then be found using L'Hospital's rule to be

$$\lim_{z \to z_0} d\vec{V}_{\mathrm{LAC}}(z_0) = \frac{\Gamma(z_0)}{4\pi} \frac{\left[0, f'''(z_0), 0\right]}{6\left(1 + f'(z_0)^2\right)^{3/2}} dz \tag{17}$$

which is finite. Therefore, in order for the total induced velocity at point z_0 to remain a finite value, $f''(z)$ must be zero in the neighborhood of z_0. This restricts the cases for which the integral in Eq. (14) is guaranteed to be convergent [4, 14, 15], and highlights one of the difficulties in generalizing the implementation of lifting-line theory.

2. Effective Bound Vortex Shape

From the requirement in Eq. (16), it appears that the only case that satisfies the condition $f''(z_0) = 0$ for every point is that of a linear locus of aerodynamic centers, as in Prandtl's classical implementation. However, by Eq (15), it is sufficient that $f''(z_0)$ equal zero only in the neighborhood of z_0, suggesting the possibility of provisionally removing the curve's concavity (i.e. force the second derivative to be zero) at a point, with minimal impact to the function at all other points. Herein, this procedure shall be referred to as *conditional concavity*. The result is an *effective locus of aerodynamic centers* for each point, z_0, along the bound vortex filament.

Consider a function defining the geometry of the bound vortex filament, $f(z)$. The line (i.e. curve whose second derivative is zero) tangent to this curve at the point z_0 is

$$f_{z_0}(z) = f'(z_0)(z - z_0) + f(z_0) \tag{18}$$

Strategically blending the original function with its tangent line will achieve the goal of conditional concavity. The blending method used in this work uses a function, $e^{-\sigma(z_0 - z)^2}$, which varies from one at z_0 to zero as $z_0 - z \to \pm\infty$. The resulting family of effective loci of aerodynamic centers can be written as

$$\tilde{f}_{z_0}(z) = \left(1 - e^{-\sigma(z_0 - z)^2}\right) f(z) + e^{-\sigma(z_0 - z)^2} \left(f'(z_0)(z - z_0) + f(z_0)\right) \tag{19}$$

with the first derivative

$$\tilde{f}'_{z_0}(z) = f'(z) + e^{-\sigma(z_0 - z)^2} \left(f'(z_0) - f'(z) - 2\sigma(z_0 - z)^2 \left(f'(z_0) - \frac{f(z_0) - f(z)}{z_0 - z} \right) \right) \tag{20}$$

where σ is a positive, real value. Adjusting σ changes the total influence of the conditional concavity on the original curve, as seen in Fig. 2. As the value of σ approaches zero, $\tilde{f}_{z_0}$ reproduces f_{z_0}, and as σ tends to infinity, $\tilde{f}_{z_0}$ yields f. The effect of σ becomes more visualizable if it is written in terms of the distance from the point z_0 at which the effective locus of aerodynamic centers is a 98.2% approximation of the original locus. This can be expressed as

$$\Delta z_{98\%} = \sqrt{\frac{-\ln(0.018)}{\sigma}} \approx \frac{2}{\sqrt{\sigma}} \tag{21}$$

This relation can be written as the following fraction of the wing's quarter-chord line, to transform the distance along the z-axis to an approximate, non-dimensional distance along the bound vortex

$$\Delta \tilde{z}_{98\%} = \frac{\Delta z_{98\%}}{b/\cos\Lambda} \approx \frac{2\cos\Lambda}{\sqrt{b^2\sigma}} \tag{22}$$

The non-dimensional distance expressed in Eq. (22) will herein be referred to as the *blending distance*. It is shown later that, for values of $\Delta\tilde{z}_{98\%}$ above a certain threshold, the lifting-line solution is insensitive to σ.

In summary, to satisfy the condition that the second derivative of the locus of aerodynamic centers be zero at the point of interest, z_0, for each spanwise location, conditional concavity is used to generate a family of effective loci of aerodynamic centers. Each locus is designed to satisfy Eq. (16) in the neighborhood of z_0, but maintain the geometry of the original curve away from the point of interest.

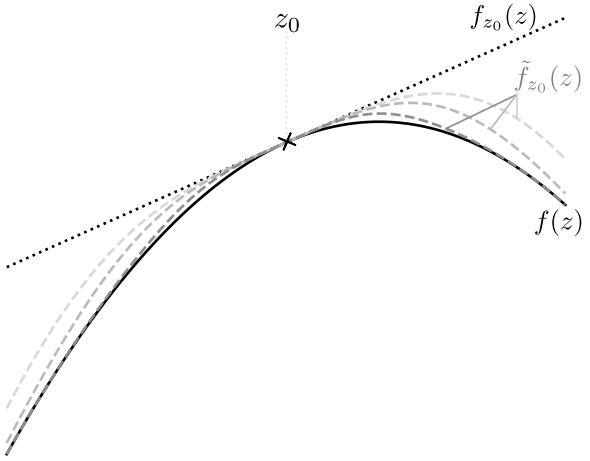

Fig. 2 An example application of conditional concavity to a parabola, $f(z)$. Several evaluations of Eq. (19), $\tilde{f}_{z_0}(z)$, are shown, each with a different value of σ, dark ($\sigma_{\max}$) to light ($\sigma_{\min}$).

B. Trailing Vortex Sheet

The velocity induced at a point by a single semi-infinite vortex is found by integrating Eq. (10) along the ray describing the vortex, resulting in the equation

$$d\vec{V} = \frac{\Gamma}{4\pi}\frac{\vec{u}_\infty \times \vec{r}}{r(r - \vec{u}_\infty \cdot \vec{r})} \tag{23}$$

where r is the magnitude of $\vec{r}$, and $\vec{u}_\infty$ is the unit vector defining the direction of the ray. The semi-infinite vortices included in the trailing vortex sheet are free vortices aligned with the freestream, so $\vec{u}_\infty$ is therefore the unit vector in the direction of the freestream velocity. The velocity induced along the locus of aerodynamic centers at z_0 by one semi-infinite vortex in the trailing vortex sheet at point z can be written as

$$d\vec{V}_{\mathrm{TV}}(z_0) = \frac{\Gamma'(z)}{4\pi}\frac{\left[u_y,\ u_z\frac{f(z_0)-f(z)}{z_0-z} - u_x,\ -u_y\frac{f(z_0)-f(z)}{z_0-z}\right]}{\left(1+\left(\frac{f(z_0)-f(z)}{z_0-z}\right)^2\right)\left(1-\frac{u_z+u_x\frac{f(z_0)-f(z)}{z_0-z}}{\sqrt{1+\left(\frac{f(z_0)-f(z)}{z_0-z}\right)^2}}\right)(z_0-z)}dz \tag{24}$$

Notice that the strength of the semi-infinite vortex is equal to the change in the circulation distribution of the bound vortex filament (i.e. $\Gamma'(z)$). The velocity induced at a point, z_0, by the entire trailing vortex sheet is then found by integrating Eq. (24) along the span of the wing, as follows

$$\vec{V}_{\mathrm{TV}}(z_0) = \int_{-b/2}^{b/2}\frac{\Gamma'(z)}{4\pi}\frac{\left[u_y,\ u_z\frac{f(z_0)-f(z)}{z_0-z} - u_x,\ -u_y\frac{f(z_0)-f(z)}{z_0-z}\right]}{\left(1+\left(\frac{f(z_0)-f(z)}{z_0-z}\right)^2\right)\left(1-\frac{u_z+u_x\frac{f(z_0)-f(z)}{z_0-z}}{\sqrt{1+\left(\frac{f(z_0)-f(z)}{z_0-z}\right)^2}}\right)(z_0-z)}dz \tag{25}$$

1. Conditions on Trailing Vortex Sheet

As was the case with the integral describing the influence of the vortex filament, given in Eq. (14), Eq. (25) also contains singularities. For example, at $z = z_0$ the limit of Eq. (24) is

$$\lim_{z\to z_0} d\vec{V}_{\mathrm{TV}}(z_0) = \frac{\Gamma'(z_0)}{4\pi}\frac{\left[u_y,\ u_z f'(z_0) - u_x,\ -u_y f'(z_0)\right]}{\left(1+f'(z_0)^2\right)\left(1-\frac{u_z+u_x f'(z_0)}{\sqrt{1+f'(z_0)^2}}\right)(z_0-z_0)}dz = \infty \tag{26}$$

which is infinite. A second singularity occurs when a slice of the trailing vortex sheet lays directly on the point at which the induced velocity is to be calculated, i.e. from the second term in the denominator of Eq. (25)

$$\frac{u_z + u_x \frac{f(z_0)-f(z)}{z_0-z}}{\sqrt{1+\left(\frac{f(z_0)-f(z)}{z_0-z}\right)^2}} = 1 \tag{27}$$

Because of the existence of singularities in the integral, neither the convergence of the integral nor the existence of its principle value can be guaranteed for an arbitrary case [4, 14, 15].

To identify conditions for which the integral can be evaluated, assume the influence of the portion of the trailing vortex sheet in the vicinity of z_0 to be adequately approximated as the influence of a semi-infinite vortex sheet of constant strength described by Hunsaker and Phillips [16] and shown in Fig. 3.

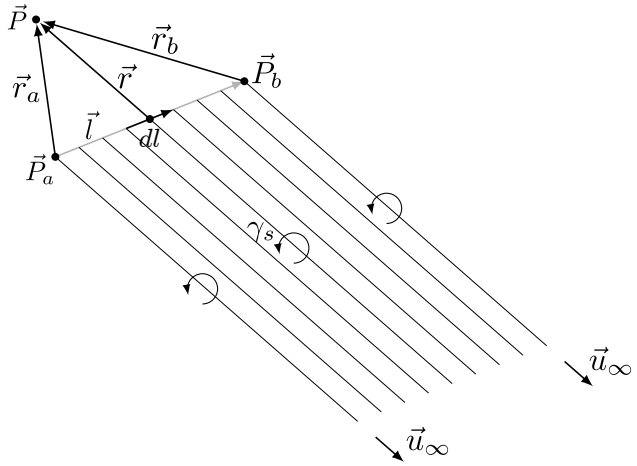

Fig. 3 The velocity induced at a point by a semi-infinite vortex sheet of constant strength.

In the case that the point at which the influence is being calculated, $\vec{P}$, is located on the line $\vec{l} = \vec{P}_b - \vec{P}_a$, such that

$$\vec{P} = \vec{P}_a + \xi\vec{l} \tag{28}$$

where $\xi \in \mathbb{R}$ is a dimensionless distance along $\vec{l}$, the vector $\vec{r}$ is defined as

$$\vec{r} = (\xi - \zeta)\vec{l} \tag{29}$$

with magnitude

$$r = |\xi - \zeta| l \tag{30}$$

where ζ is a dimensionless distance along $\vec{l}$ from $\vec{P}_a$ to $\vec{P}_b$, such that $0 < \zeta < 1$. The influence on such a point can be described by the integral

$$\begin{aligned}\vec{V}_s &= \frac{\gamma_s l}{4\pi}\int_0^1 \frac{(\xi-\zeta)(\vec{u}_\infty \times \vec{l})}{|\xi-\zeta| l\Big(|\xi-\zeta| l - (\xi-\zeta)(\vec{u}_\infty \cdot \vec{l})\Big)} d\zeta \\ &= \frac{\gamma_s l}{4\pi}\int_0^1 \frac{\text{sign}(\xi-\zeta)(\vec{u}_\infty \times \vec{l})}{l\Big(l - \text{sign}(\xi-\zeta)(\vec{u}_\infty \cdot \vec{l})\Big)|\xi-\zeta|} d\zeta\end{aligned} \tag{31}$$

which can be evaluated to give

$$\vec{V}_s = \frac{\gamma_s l}{4\pi} \begin{cases} \int_0^1 \frac{-(\vec{u}_\infty \times \vec{l})}{l\left(l+(\vec{u}_\infty \cdot \vec{l})\right)(-\xi+\zeta)} d\zeta & \xi < 0 \\ \lim_{\epsilon \to 0^+} \left[\int_0^{\xi-\epsilon} \frac{(\vec{u}_\infty \times \vec{l})}{l\left(l-(\vec{u}_\infty \cdot \vec{l})\right)(\xi-\zeta)} d\zeta + \int_{\xi+\epsilon}^1 \frac{-(\vec{u}_\infty \times \vec{l})}{l\left(l+(\vec{u}_\infty \cdot \vec{l})\right)(-\xi+\zeta)} d\zeta \right] & 0 < \xi < 1 \\ \int_0^1 \frac{(\vec{u}_\infty \times \vec{l})}{l\left(l-(\vec{u}_\infty \cdot \vec{l})\right)(\xi-\zeta)} d\zeta & 1 < \xi \end{cases} \tag{32}$$

In the case that $0 < \xi < 1$, it is only when $\vec{u}_\infty \cdot \vec{l} = 0$ that the principle value of the integral exists. The total influence of the sheet in this case can thus be written

$$\vec{V}_s = \frac{\gamma_s l}{4\pi} \begin{cases} \frac{(\vec{u}_\infty \times \vec{l})}{l\left(l+(\vec{u}_\infty \cdot \vec{l})\right)} \ln\left(\frac{\xi}{\xi-1}\right) & \xi < 0 \\ \begin{cases} \frac{(\vec{u}_\infty \times \vec{l})}{l^2} \ln\left(\frac{\xi}{\xi-1}\right) & \text{if } \vec{u}_\infty \cdot \vec{l} = 0 \\ \text{undefined} & \text{if } \vec{u}_\infty \cdot \vec{l} \neq 0 \end{cases} & 0 < \xi < 1 \\ \frac{(\vec{u}_\infty \times \vec{l})}{l\left(l-(\vec{u}_\infty \cdot \vec{l})\right)} \ln\left(\frac{\xi}{\xi-1}\right) & 1 < \xi \end{cases} \tag{33}$$

where only the real part of the complex influence is considered in the case that $0 < \xi < 1$ and $\vec{u}_\infty \cdot \vec{l} = 0$.

The case of this semi-infinite vortex sheet of constant strength can be extended to hypothesize about the case in which the influence of a general trailing vortex sheet on the point z_0 may be evaluated. It is thus presumed that, in order for the total induced velocity at point z_0 to remain definite, the condition

$$\vec{r}_\delta(z_0) \perp \vec{r}(z) \tag{34}$$

must exist in the neighborhood of z_0. The validity of this conjecture is shown later in this work, so long as δ/c is above a certain threshold.

Prandtl's classical implementation of lifting-line theory again inherently satisfies the requirement that a trailing vortex sheet must be perpendicular to $f(z)$ at the point of interest, by restricting the linear locus of aerodynamic centers to freestream conditions without sideslip. Thus, the line representing the locus of aerodynamic centers is at all points perpendicular to the trailing vortex sheet.

2. Jointed Trailing Vortex Sheet

To allow for a more general locus of aerodynamic center shape and freestream conditions, the classic trailing vortex sheet used in Prandtl's lifting-line implementation must be modified. One simple modification is made by *jointing* each trailing vortex, such that there is a finite segment of the trailing vortex perpendicular to, and in the same plane as, $f(z)$, and a semi-infinite portion aligned with the freestream, as seen in Fig. 4.

Using the notation in Fig. 4, the velocity induced at a point by the finite segment of the jointed vortex can be described by integrating Eq. (10) along $\vec{r}_\delta$, to give

$$d\vec{V}_\delta(z_0) = \frac{\Gamma'(z)}{4\pi} \frac{(r + |\vec{r} - \vec{r}_\delta|)(\vec{r} \times (\vec{r} - \vec{r}_\delta))}{r|\vec{r} - \vec{r}_\delta|(r|\vec{r} - \vec{r}_\delta| + \vec{r} \cdot (\vec{r} - \vec{r}_\delta))} \tag{35}$$

where

$$\vec{r} = \left[f(z_0) - f(z), 0, z_0 - z \right] \tag{36}$$

and

$$\vec{r}_\delta = \left[1, 0, -f'(z_b) \right] \frac{\delta}{\sqrt{1 + f'(z_b)^2}} \tag{37}$$

where δ is the length of the finite vortex segment. Herein, this length is most often written as a fraction of the local chord, δ/c. Similarly, the velocity induced at a point by the semi-infinite portion of the trailing vortex can be described by Eq. (23) as

$$d\vec{V}_{\mathrm{TV}'}(z_0) = \frac{\Gamma'(z)}{4\pi} \frac{\vec{u}_\infty \times (\vec{r} - \vec{r}_\delta)}{|\vec{r} - \vec{r}_\delta|(|\vec{r} - \vec{r}_\delta| - \vec{u}_\infty \cdot (\vec{r} - \vec{r}_\delta))} \tag{38}$$

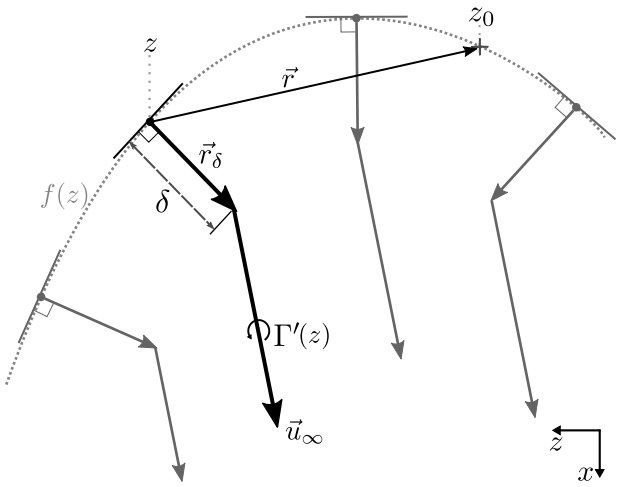

Fig. 4 The velocity induced at a point by a single semi-infinite, jointed vortex.

where $\vec{u}_\infty$ is the unit vector pointing in the direction of the freestream

$$\vec{u}_\infty = \left[u_x, u_y, u_z\right] \tag{39}$$

Thus, the total velocity induced at a point, z_0, is found by integrating the influence of the sheet of finite segments and the influence of the sheet of semi-infinite vortices along z

$$\begin{aligned}\vec{V}_{\mathrm{TV}_\delta}(z_0) &= \int_{-b/2}^{b/2} \left(d\vec{V}_\delta(z_0) + d\vec{V}_{\mathrm{TV}'}(z_0)\right) dz \\ &= \int_{-b/2}^{b/2} \frac{\Gamma'(z)}{4\pi} \left(\frac{(r + |\vec{r} - \vec{r}_\delta|)(\vec{r} \times (\vec{r} - \vec{r}_\delta))}{r|\vec{r} - \vec{r}_\delta|(r|\vec{r} - \vec{r}_\delta| + \vec{r} \cdot (\vec{r} - \vec{r}_\delta))} + \frac{\vec{u}_\infty \times (\vec{r} - \vec{r}_\delta)}{|\vec{r} - \vec{r}_\delta|(|\vec{r} - \vec{r}_\delta| - \vec{u}_\infty \cdot (\vec{r} - \vec{r}_\delta))} \right) dz \end{aligned} \tag{40}$$

Notice that, as $z \to z_0$, only the first term in the integral is indeterminate—due to r in the denominator approaching zero. If the region near z_0 is sufficiently similar to the semi-infinite vortex sheet of constant strength described in Section II.B.1, the principle value of this integral will exist despite the asymptotic behavior of the function being integrated. This conjecture will be validated in its application hereafter.

C. Total Induced Velocity

Combining the integrals for the velocity induced by the trailing vortex sheet given in Eq (40) and the bound vorticity given in Eq (14) results in the total velocity induced at the point z_0

$$\vec{V}_i(z_0) = \int_{-b/2}^{b/2} \left(d\vec{V}_{\mathrm{LAC}}(z_0) + d\vec{V}_{\mathrm{TV}_\delta}(z_0)\right) dz \tag{41}$$

As discussed in the previous sections, this integral contains singularities that can cause the integral to diverge. However, convergence of the integral can be assured if, in the neighborhood of z_0, the conditions in Eq. 16, i.e.

$$f''(z_0) = 0$$

and Eq. 34, i.e.

$$\vec{r}_\delta(z_0) \perp \vec{r}(z)$$

are met. The resulting model for the velocity induced at a point, as given in Eq. (41), can now be used in the implementation of a general lifting-line theory.

III. Additional Considerations for a General Lifting-Line Implementation

In addition to the special consideration that must be given to the evaluation of the velocity induced by the bound vortex filament and the trailing vortex sheet, consideration must be given to modeling the locus of aerodynamic centers of non-straight wings, and the section aerodynamic properties of such wings. This work focuses exclusively on planar wings, with a focus on the effect of wing sweep, but the concepts described heretofore and hereafter lend themselves to straightforward extension to non-planar wings.

A. Swept Wing Locus of Aerodynamic Centers

When a wing is swept, the locus of aerodynamic centers becomes curved at the root and tip. In his 1956 paper, Küchemann modeled the shift in aerodynamic center from the quarter-chord along a wing of constant sweep, taking into account aspect ratio effects [17]. To account for the effects of aspect ratio, Küchemann defines an effective global wing sweep angle

$$\Lambda_K = \frac{\Lambda_w}{\left(1 + \left(\frac{\tilde{C}_{L,\alpha} \cos \Lambda_w}{\pi R_A}\right)^2\right)^{1/4}} \tag{42}$$

where Λ_w is the global sweep of the wing, $\tilde{C}_{L,\alpha}$ is the lift slope of the root airfoil, and R_A is the aspect ratio of the wing. Using Λ_K, Küchemann then approximates the locus of aerodynamic centers with the function

$$f(z) = \frac{1}{4}c(0) + |z| \tan \Lambda_w - \frac{c(z)}{4}\left(1 - \frac{1}{K}\left(1 + 2\lambda(z)\frac{\Lambda_K}{\pi}\right)\right) \tag{43}$$

where

$$K = \left(1 + \left(\frac{\tilde{C}_{L,\alpha} \cos \Lambda_K}{\pi R_A}\right)^2\right)^{\frac{\pi}{4(\pi + 2|\Lambda_K|)}} \tag{44}$$

and $\lambda(z)$ is the hyperbolic interpolation function

$$\begin{aligned}\lambda(z) =& \left(\sqrt{1 + \left(2\pi \frac{\tan \Lambda_K}{\Lambda_K} \frac{z}{c(z)}\right)^2} - 2\pi \frac{\tan \Lambda_K}{\Lambda_K} \frac{|z|}{c(z)}\right)_{center} \\ &- \left(\sqrt{1 + \left(2\pi \frac{\tan \Lambda_K}{\Lambda_K} \frac{\frac{b}{2} - |z|}{c(z)}\right)^2} - 2\pi \frac{\tan \Lambda_K}{\Lambda_K} \frac{\frac{b}{2} - |z|}{c(z)}\right)_{tips}\end{aligned} \tag{45}$$

The first term on the right hand side of Eq. (45) describes the effect of the wing center on the locus of aerodynamic centers, and the second term describes the effect of the wing tips. The first derivative of the locus of aerodynamic centers must be known to calculate the effective locus of aerodynamic centers as well as the jointed trailing vortices. The first derivative of Eq. (43) is

$$f'(z) = \frac{z}{|z|} \tan \Lambda_w + \lambda'(z) \frac{\Lambda_K}{2\pi} \frac{c(z)}{K} - \frac{c'(z)}{4}\left(1 - \frac{1}{K}\left(1 + 2\lambda(z)\frac{\Lambda_K}{\pi}\right)\right) \tag{46}$$

where

$$\begin{aligned}\lambda'(z) =& \left(\frac{4\pi^2 \frac{\tan^2 \Lambda_K}{\Lambda_K^2}\left(zc(z) - z^2 c'(z)\right)}{c(z)^3 \sqrt{1 + \left(2\pi \frac{\tan \Lambda_K}{\Lambda_K} \frac{z}{c(z)}\right)^2}} - 2\pi \frac{\tan \Lambda_K}{\Lambda_K} \frac{\frac{z}{|z|}c(z) - |z|c'(z)}{c(z)^2}\right)_{center} \\ &+ \left(\frac{4\pi^2 \frac{\tan^2 \Lambda_K}{\Lambda_K^2}\left(\frac{z}{|z|}(\frac{b}{2} - |z|)c(z) + (\frac{b}{2} - |z|)^2 c'(z)\right)}{c(z)^3 \sqrt{1 + \left(2\pi \frac{\tan \Lambda_K}{\Lambda_K} \frac{\frac{b}{2} - |z|}{c(z)}\right)^2}} - 2\pi \frac{\tan \Lambda_K}{\Lambda_K} \frac{\frac{z}{|z|}c(z) + (\frac{b}{2} - |z|)c'(z)}{c(z)^2}\right)_{tips}\end{aligned} \tag{47}$$

The results of lifting-line theory are likely dependent on the model used for the locus of aerodynamic centers. However, Eq. (43) has been proven sufficiently accurate by Moorthamers and Hunsaker [18], and such sensitivity is not to be explored in this work.

B. Swept Wing Section Data

As mentioned in the introduction, lifting-line theory requires knowledge of section properties. The section aerodynamic properties and the effective flow properties of swept wing sections differ from the those of straight wings [19]. Slices of the wing are taken normal to the locus of aerodynamic centers, $f(z)$, such that each section of the wing has a local, effective sweep angle, defined by the locus of aerodynamic centers as

$$\Lambda(z) = -\tan^{-1}\left(f'(z)\right) \tag{48}$$

Note that, for this definition of effective sweep angle, a negative effective sweep results for wing sections that correlate to a left-hand infinite wing (i.e. an infinite wing in a coordinate system mirroring the one used herein). This sign change is important in accounting for the effective sideslip experienced by a section. Given a local angle of sweep, Λ, local angle of attack, α, and local sideslip angle, β, the effective freestream velocity magnitude, angle of attack, and sideslip angle, for a given section, are described as [19]

$$V_{\infty_\Lambda} = V_\infty \frac{\sqrt{\cos^2\alpha\cos^2(\Lambda-\beta) + \sin^2\alpha\cos^2\beta}}{\sqrt{1-\sin^2\alpha\sin^2\beta}} \tag{49}$$

$$\alpha_\Lambda = \tan^{-1}\left(\frac{\tan\alpha\cos\beta}{\cos(\Lambda-\beta)}\right) \tag{50}$$

$$\beta_\Lambda = \beta - \Lambda \tag{51}$$

Similarly, a section of a swept wing has an effective airfoil geometry that is found by slicing the wing in the plane normal to the locus of aerodynamic centers, which has the effect of scaling the chordwise coordinates of the airfoil by the cosine of the local sweep angle, as seen in Fig. 5.

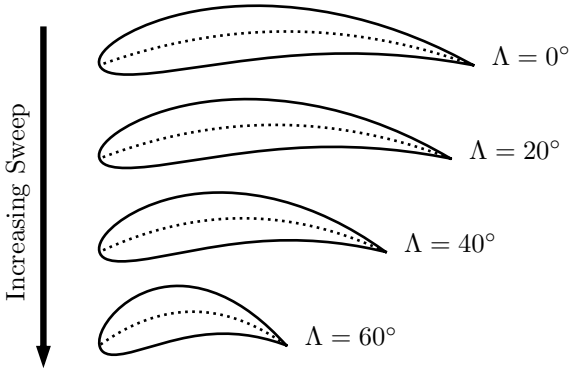

Fig. 5 The change in effective airfoil geometry with sweep.

Given the effective sweep angle, the effective freestream velocity magnitude and angle of attack are found for the section, along with the circulation produced by the effective airfoil geometry, Γ_Λ. Applying the effecive freestream velocity magnitude from Eq. (49) to Eq. (1), the section lift coefficient for a wing section can be rewritten as

$$\tilde{C}_{L_\Lambda} = \frac{2V_{\infty_\Lambda}\Gamma_\Lambda}{V_\infty^2 c\cos\Lambda} = \frac{\sqrt{\cos^2\alpha\cos^2(\Lambda-\beta) + \sin^2\alpha\cos^2\beta}}{\sqrt{1-\sin^2\alpha\sin^2\beta}} \frac{2\Gamma_\Lambda}{V_\infty c\cos\Lambda} \tag{52}$$

where Γ_Λ is the circulation produced by the corresponding effective airfoil geometry. The amount of circulation produced by the effective airfoil geometry may be approximated through inviscid prediction methods, simulations that take into account viscous effects, or experimental data. Herein, Γ_Λ is predicted by the equation

$$\Gamma_\Lambda = \frac{\cos\beta_\Lambda(\alpha_\Lambda - \alpha_{L0_\Lambda})}{\sqrt{1-\sin^2\alpha_\Lambda\sin^2\beta_\Lambda}}\Gamma_{\Lambda,\alpha_\Lambda} \tag{53}$$

where $\Gamma_{\Lambda,\alpha_\Lambda}$ is the change in the section circulation, Γ_Λ, with respect to the effective angle of attack, α_Λ, and α_{L0_Λ} is the effective angle of attack that results in zero section circulation.

Both $\Gamma_{\Lambda,\alpha_\Lambda}$ and α_{L0_Λ} may be found by analyzing an infinite wing with no sweep, whose airfoil section is the effective airfoil section of the swept section. Varying the angle of attack of such an infinite wing (while maintaining zero sideslip) results in a circulation curve from which $\Gamma_{\Lambda,\alpha_\Lambda}$ and α_{L0_Λ} can be extracted. A non-dimensionalized form of $\Gamma_{\Lambda,\alpha_\Lambda}$ can be written as

$$\tilde{C}_{L_{\Lambda,\alpha_\Lambda}} = \frac{2\Gamma_{\Lambda,\alpha_\Lambda}}{V_\infty c \cos\Lambda} \tag{54}$$

The section lift coefficient for a wing section, defined in Eq. (52), can be rewritten as

$$\tilde{C}_{L_\Lambda} = \frac{\sqrt{\cos^2\alpha\cos^2(\Lambda-\beta)+\sin^2\alpha\cos^2\beta}}{\sqrt{1-\sin^2\alpha\sin^2\beta}} \frac{\cos\beta_\Lambda}{\sqrt{1-\sin^2\alpha_\Lambda\sin^2\beta_\Lambda}} \tilde{C}_{L_{\Lambda,\alpha_\Lambda}}\left(\alpha_\Lambda - \alpha_{L0_\Lambda}\right) \tag{55}$$

If the sweep angle is small, $\tilde{C}_{L_{\Lambda,\alpha_\Lambda}}$ and α_{L0_Λ} may be approximated by $\tilde{C}_{L,\alpha}$ and α_{L0}.

IV. General Implementation of Lifting-Line Theory

Having considered the velocity induced along the locus of aerodynamic centers, the shape of the locus of aerodynamic centers itself for wings with sweep, and the section properties of swept wings, a more general implementation of lifting-line theory can be developed. Following Prandtl's original methodology in Eqs. (1) through (9), but allowing for generalizations of freestream direction and wing geometry, an analytic implementation is discussed. Due to the mathematical complexity of the resulting analytical implementation the advantages of a numerical implementation are also examined.

A. General, Analytic Lifting-Line Theory Implementation

As previously discussed, the velocity induced at a point, z_0, along the locus of aerodynamic centers is characterized by Eq. (41) as

$$\vec{V}_i(z_0) = \int_{-b/2}^{b/2} \left(d\vec{V}_{\mathrm{LAC}}(z_0) + d\vec{V}_{\mathrm{TV}_\delta}(z_0)\right) dz$$

which is the sum of the influences of the bound vortex filament and the jointed trailing vortex sheet. The local velocity at z_0 is thus the sum of the freestream velocity and the induced velocity

$$\vec{V}(z_0) = \vec{V}_\infty + \vec{V}_i(z_0) = \left[V_{\infty_x} + V_{i_x}(z_0),\ V_{\infty_y} + V_{i_y}(z_0),\ V_{\infty_z} + V_{i_z}(z_0)\right] \tag{56}$$

Using Eq. (51), the effective angle of attack for each spanwise section can be written as

$$\alpha_{\mathrm{eff}}(z_0) = \tan^{-1}\left(\frac{\tan\alpha_i(z_0)\cos\beta_i(z_0)}{\cos\left(\Lambda(z_0)-\beta_i(z_0)\right)}\right) \tag{57}$$

where

$$\alpha_i(z_0) = \tan^{-1}\left(\frac{V_{\infty_y} + V_{i_y}(z_0)}{V_{\infty_x} + V_{i_x}(z_0)}\right) \tag{58}$$

$$\beta_i(z_0) = \tan^{-1}\left(\frac{V_{\infty_z} + V_{i_z}(z_0)}{V_{\infty_x} + V_{i_x}(z_0)}\right) \tag{59}$$

Rearranging, the effective angle of attack in Eq. (57) can be expressed in the form

$$\alpha_{\mathrm{eff}}(z_0) = \tan^{-1}\left(\frac{V_{\infty_y} + V_{i_y}(z_0)}{\left(V_{\infty_x} + V_{i_x}(z_0)\right)\cos\Lambda(z_0) + \left(V_{\infty_z} + V_{i_z}(z_0)\right)\sin\Lambda(z_0)}\right) \tag{60}$$

With an expression for the effective angle of attack, a formulation similar to Prandtl's can be obtained.

The lift coefficient produced by each swept section can be modeled as a linear function of angle of attack

$$\tilde{C}_{L_\Lambda}(z_0) = \tilde{C}_{L_\Lambda,\alpha}(z_0)\left(\alpha_{\mathrm{eff}}(z_0) - \alpha_{L0_\Lambda}(z_0)\right) \tag{61}$$

where $\tilde{C}_{L_\Lambda,\alpha}$ is the lift slope of the effective airfoil [19]. The section lift coefficient is also related to the local circulation by the Kutta-Joukowski theorem

$$\tilde{C}_{L_\Lambda}(z_0) = R_\Lambda \frac{2\Gamma(z_0)}{V_\infty c(z_0)} \tag{62}$$

with

$$R_\Lambda = \frac{\sqrt{\cos^2\alpha\cos^2(\Lambda(z_0)-\beta)+\sin^2\alpha\cos^2\beta}}{\cos\Lambda(z_0)\sqrt{1-\sin^2\alpha\sin^2\beta}}$$

where α and β are the local aerodynamic angles of the wing. Equating Eq. (61) and Eq. (62), and using the definition for α_{eff} in Eq. (60) yields

$$\tan^{-1}\left(\frac{V_{\infty_y}+V_{i_y}(z_0)}{(V_{\infty_x}+V_{i_x}(z_0))\cos\Lambda(z_0)+(V_{\infty_z}+V_{i_z}(z_0))\sin\Lambda(z_0)}\right)-\alpha_{L0_\Lambda}(z_0) = R_\Lambda\frac{2\Gamma(z_0)}{\tilde{C}_{L_\Lambda,\alpha}(z_0)V_\infty c(z_0)} \tag{63}$$

where V_{i_x}, V_{i_y}, and V_{i_z} are also functions of the circulation distribution, $\Gamma(z)$. As in Prandtl's implementation, the change of variables defined by Eqs. (5) and (6) can be used to express $\Gamma(z)$ as the Fourier sine series shown in Eqs. (7) and (8). To determine the Fourier coefficients, A_n, Eq. (63) is evaluated at N control points along the wing, resulting in a system of N non-linear equations to be solved, after performing the integration necessary to determine the induced velocity, $\vec{V}_i$.

For computational simplicity, it is desirable to have a system of linear equations to solve, similar to that obtained by Prandtl's classical lifting-line implementation. Assuming that α_{eff} is small and that V_{i_y} is the only non-negligible component of the induced velocity, as did Prandtl, the effective angle of attack described in Eq. (60) can be written as

$$\alpha_{\text{eff}}(z_0) \approx \frac{V_{\infty_y}+V_{i_y}(z_0)}{V_{\infty_x}\cos\Lambda(z_0)+V_{\infty_z}\sin\Lambda(z_0)} \tag{64}$$

and Eq. (63) becomes

$$\frac{V_{\infty_y}+V_{i_y}(z_0)}{V_{\infty_x}\cos\Lambda(z_0)+V_{\infty_z}\sin\Lambda(z_0)}-\alpha_{L0_\Lambda}(z_0) = R_\Lambda\frac{2\Gamma(z_0)}{\tilde{C}_{L_\Lambda,\alpha}(z_0)V_\infty c(z_0)} \tag{65}$$

where

$$V_{i_y}(z_0) = \int_{-b/2}^{b/2}\left(dV_{\text{LAC}_y}(z_0)+dV_{\text{TV}_{\delta y}}(z_0)\right)dz \tag{66}$$

Equation (65) can be rewritten in terms of θ using Eqs. (5) - (8), yielding

$$\begin{aligned}&\frac{V_{\infty_y}}{V_{\infty_x}\cos\Lambda(\theta_0)+V_{\infty_z}\sin\Lambda(\theta_0)}-\alpha_{L0_\Lambda}(\theta_0)\\ &\quad= 2bV_\infty\sum_1^N A_n\left(\frac{2R_\Lambda\sin(n\theta_0)}{\tilde{C}_{L_\Lambda,\alpha}(\theta_0)V_\infty c(\theta_0)}-\frac{\int_0^\pi\left(\frac{b}{2}\sin(\theta)\sin(n\theta)\frac{dV_{\text{LAC}_y}(\theta_0)}{\Gamma(\theta)}+n\cos(n\theta)\frac{dV_{\text{TV}_{\delta y}}(\theta_0)}{\Gamma'(\theta)}\right)d\theta}{V_{\infty_x}\cos\Lambda(\theta_0)+V_{\infty_z}\sin\Lambda(\theta_0)}\right)\end{aligned} \tag{67}$$

Now, when Eq. (67) is evaluated at N control points along the wing, the result is a linear system of N equations whose solution is the Fourier coefficients, A_n.

Consider a simple case of Eq. (67), specifically, a straight wing in side-slip at an angle of attack of zero degrees. In this case, the locus of aerodynamic centers is approximated as a line along the z-axis ($f(z) = 0, f'(z) = 0$). Thus, the bound vortex filament induces no velocity along the locus of aerodynamic centers, $dV_{\text{LAC}_y} = 0$, and Eq. (67) becomes

$$\begin{aligned}&\frac{V_{\infty_y}}{V_{\infty_x}\cos\Lambda(\theta_0)+V_{\infty_z}\sin\Lambda(\theta_0)}-\alpha_{L0_\Lambda}(\theta_0)\\ &\quad= 2bV_\infty\sum_1^N A_n\left(\frac{2\cos(\beta)\sin(n\theta_0)}{\tilde{C}_{L_\Lambda,\alpha}(\theta_0)V_\infty c(\theta_0)}-\frac{\frac{n}{4\pi}\int_0^\pi\frac{\cos(n\theta)}{|\vec{r}-\vec{r}_\delta|}\left(\frac{\delta}{r}-\frac{u_z\delta+u_x\frac{b}{2}\left(\cos(\theta)-\cos(\theta_0)\right)}{\left(|\vec{r}-\vec{r}_\delta|-u_z\frac{b}{2}\left(\cos(\theta)-\cos(\theta_0)\right)+u_x\delta\right)}\right)d\theta}{V_{\infty_x}\cos\Lambda(\theta_0)+V_{\infty_z}\sin\Lambda(\theta_0)}\right)\end{aligned} \tag{68}$$

where

$$r = \frac{b}{2}|\cos(\theta) - \cos(\theta_0)| \tag{69}$$

$$|\vec{r} - \vec{r}_\delta| = \sqrt{\frac{b^2}{4}(\cos(\theta) - \cos(\theta_0))^2 + \delta^2} \tag{70}$$

Ideally, this equation would yield a closed-form solution, as for the case of a straight wing with no sideslip. However, the integral in the second term of the right-hand side of Eq. (68) is beyond the scope of traditional integration methods, and, because of the singularity contained within the bounds of integration, numerical evaluation of that integral does not yield usable results. Even using techniques to improve its numerical behavior, the integral does not have good numerical performance [20]. Instead, the general considerations for the velocity induced along the locus of aerodynamic centers, the shape of the locus of aerodynamic centers itself, and the section properties of swept wings will be applied to a numerical implementation of lifting-line theory, first developed by Phillips [3, 11], since the numerical implementation does not require integration, as shown hereafter.

B. General, Numerical Lifting-Line Theory Implementation

The numerical implementation of lifting-line theory developed by Phillips will be the foundation for the general lifting-line theory implementation [3, 11]. Phillips' implementation separates the bound vortex filament and trailing vortex sheet into a discrete number of abutted *horseshoe vortices*, each consisting of a constant-strength vortex segment and two semi-infinite vortices, shown in Fig. 6. Endpoints of the bound portion of each horseshoe vortex lay on the wing's locus of aerodynamic centers, and the trailing portion of each horseshoe vortex is aligned with the freestream. The local velocity is calculated at a control point located on each bound vortex segment with the equation

$$\vec{V}_i = \vec{V}_\infty + \sum_{j=1}^{N} \Gamma_j \vec{v}_{ji} \tag{71}$$

where Γ_j is the strength of each horseshoe vortex, and $\vec{v}_{ji}$ is the influence of vortex j on control point i.

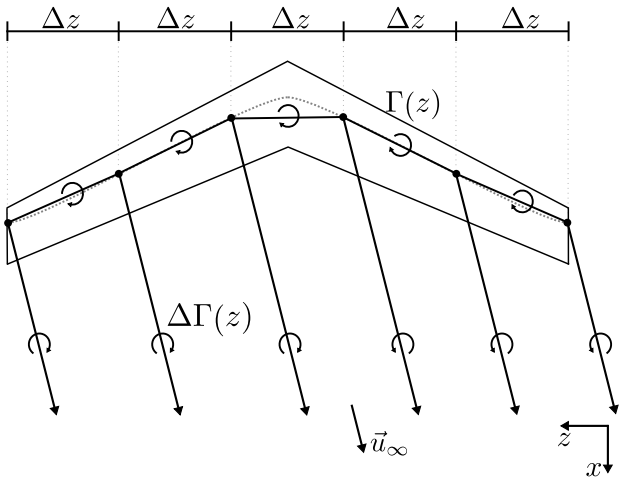

Fig. 6 A wing whose circulation is approximated by a finite number of horseshoe vortices. The bound portion of each horseshoe vortex is collocated on the wing's locus of aerodynamic centers with a spacing, Δz, along the z-axis. The trailing portion of each horseshoe vortex is aligned with the freestream.

Similar to Prandtl's implementation, each circulation, Γ_j, is not initially known, but is determined by relating two definitions of the force generated by each section of the wing. Using the vectorized form of the Kutta-Joukowski law, the force that each bound vortex exerts, given a local velocity vector, $\vec{V}_i$, can be described by the equation

$$d\vec{F}_i = \rho \Gamma_i \vec{V}_i \times d\vec{l}_i \tag{72}$$

This definition for section force is related to information obtained from an analytic, numerical, empirical, or experimental prediction of the section lift coefficient as a function of the local velocity, $\tilde{C}_L(\vec{V}_i)$. Using Eq. (71) in Eq. (72), and equating the result to the section lift coefficient, gives a non-linear system of equations which can be solved iteratively

$$\rho\Gamma_i \left| \left(\vec{V}_\infty + \sum_{j=1}^{N} \Gamma_j \, \vec{v}_{ji} \right) \times d\vec{l}_i \right| - \frac{1}{2}\rho V_\infty^2 \tilde{C}_L(\vec{V}_i) dA_i = 0 \tag{73}$$

It is convenient to rewrite Eq. (73) in the non-dimensionalized form

$$2 \left| \left(\vec{u}_\infty + \sum_{j=1}^{N} G_j \, \vec{v}_{ji} \right) \times \vec{\zeta}_i \right| G_i - \tilde{C}_L(\vec{V}_i) = 0 \tag{74}$$

where

$$\vec{u}_\infty = \frac{\vec{V}_\infty}{V_\infty}, \quad G_i = \frac{\Gamma_i}{V_\infty}, \quad \vec{\zeta}_i = \frac{d\vec{l}_i}{dA_i} \tag{75}$$

Solving this non-linear system for G_i provides the circulation distribution of the wing, and the lift distribution is then found from Eqs. (71) and (72).

The discrete number of horseshoe vortices shown in Fig. 6 are spaced by Δz along the z-axis. Before discussing the generalization of this numerical implementation of lifting-line theory, the limit as the number of these vortices increases to infinity (i.e. $\Delta z \to 0$) is considered.

1. Limit of Bound Vortex Segments

Using the notation in Fig. 7, the velocity induced at a point by a single linear vortex segment can be described as

$$d\vec{V}_2 = \frac{\Gamma_1}{4\pi} \frac{(r_1 + r_2)(\vec{r}_1 \times \vec{r}_2)}{r_1 r_2 (r_1 r_2 + \vec{r}_1 \cdot \vec{r}_2)} \tag{76}$$

where r_1 and r_2 are the magnitudes of $\vec{r}_1$ and $\vec{r}_2$. Using point b as a reference, the vectors $\vec{r}_1$ and $\vec{r}_2$ are defined as

$$\vec{r}_1 = \left[\frac{f(z_c) + f(z_c - \Delta z)}{2} - f(z_b + \Delta z), 0, -z - \frac{3\Delta z}{2} \right] \tag{77}$$

$$\vec{r}_2 = \left[\frac{f(z_c) + f(z_c - \Delta z)}{2} - f(z_b), 0, -z - \frac{\Delta z}{2} \right] \tag{78}$$

As $\Delta z \to 0$, Eq. (76) becomes

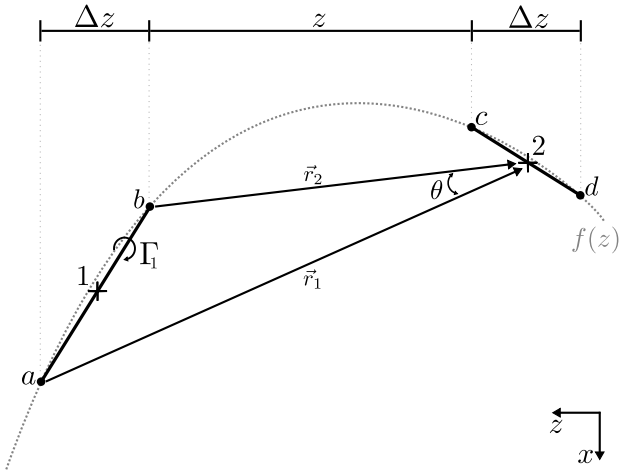

Fig. 7 The velocity induced at a point by a single linear vortex segment. ($\Delta z > 0$ **and** $z = z_b - z_c$)

$$\lim_{\Delta z\to 0} d\vec{V}_2 = \lim_{\Delta z\to 0} \frac{\Gamma(z_b+\frac{\Delta z}{2})}{4\pi} \frac{(r_1+r_2)\Big[0, -\frac{f(z_c)+f(z_c-\Delta z)}{2} + \frac{3f(z_b)-f(z_b+\Delta z)}{2} + z\frac{f(z_b)-f(z_b+\Delta z)}{\Delta z}, 0\Big]\Delta z}{r_1 r_2(r_1 r_2 + \vec{r}_1\cdot\vec{r}_2)}$$
$$= \frac{-\Gamma(z_b)}{4\pi} \frac{\Big[0, \frac{f(z_c)-f(z_b)}{z} + f'(z_b), 0\Big]}{\Big(1+\Big(\frac{f(z_c)-f(z_b)}{z}\Big)^2\Big)^{3/2} z^2} dz \tag{79}$$

which is of the same form as the velocity induced by the continuous bound vortex seen in Eq. (13). Thus, as the number of discrete vortex segments increases to infinity, the behavior of the continuous, bound vortex filament is achieved. Therefore, it can be expected that Phillips' implementation suffers the same shortcomings as Prandtl's as $z \to 0$, when modeling a wing with a non-linear locus of aerodynamic centers.

2. Limit of Trailing Semi-Infinite Vortices

Using the notation in Fig. 8, the velocity induced at a point by a single semi-infinite vortex can be described as

$$d\vec{V}_3 = \frac{\Gamma_b}{4\pi} \frac{\vec{u}_\infty \times \vec{r}_b}{r_b(r_b - \vec{u}_\infty\cdot\vec{r}_b)} \tag{80}$$

where r_b is the magnitude of $\vec{r}_b$. Using point b as a reference, the vectors $\vec{u}_\infty$ and $\vec{r}_b$ are defined as

$$\vec{u}_\infty = \Big[u_x, u_y, u_z\Big] \tag{81}$$

$$\vec{r}_b = \Big[\frac{f(z_d)+f(z_d-\Delta z)}{2} - f(z_b), 0, -(z_b - z_d) - \frac{\Delta z}{2}\Big] \tag{82}$$

and Γ_b is defined as

$$\Gamma_b = \Gamma_1 - \Gamma_2 = \Gamma\Big(z_b + \frac{\Delta z}{2}\Big) - \Gamma\Big(z_b - \frac{\Delta z}{2}\Big) \tag{83}$$

As $\Delta z \to 0$, Eq. (80) becomes

$$\lim_{\Delta z\to 0} \vec{v}_3 = \lim_{\Delta z\to 0} \frac{\Gamma\Big(z_b+\frac{\Delta z}{2}\Big) - \Gamma\Big(z_b-\frac{\Delta z}{2}\Big)}{4\pi\Delta z} \frac{\vec{u}_\infty\times\vec{r}_b}{r_b(r_b-\vec{u}_\infty\cdot\vec{r}_b)}\Delta z$$
$$= \frac{\Gamma'(z_b)}{4\pi} \frac{\Big[u_y,\ u_z\frac{f(z_d)-f(z_b)}{z_d-z_b} - u_x,\ -u_y\frac{f(z_d)-f(z_b)}{z_d-z_b}\Big]dz}{\sqrt{1+(\frac{f(z_d)-f(z_b)}{z_d-z_b})^2}\Big(\sqrt{1+(\frac{f(z_d)-f(z_b)}{z_d-z_b})^2} - u_z - u_x\frac{f(z_d)-f(z_b)}{z_d-z_b}\Big)(z_d-z_b)} \tag{84}$$

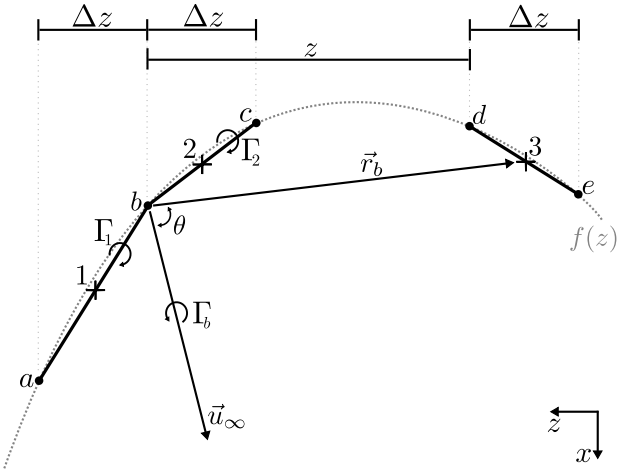

Fig. 8 The velocity induced at a point by a single semi-infinite vortex. ($\Delta z > 0$ and $z = z_b - z_d$)

which matches Eq. (24), the influence of an infinitesimal slice of a vortex sheet with width dz, and shows that a discrete number of semi-infinite vortices replicate the behavior of a vortex sheet, like that used by Prandtl, as the number of discrete vortices approaches infinity. As previously discussed, the velocity induced by a vortex sheet can only be found in the case that the freestream is perpendicular to $\vec{r}(z)$. As such, it is anticipated that Phillips' numerical implementation is restricted to cases wherein $\vec{u}_\infty$ is perpendicular to $\vec{r}(z)$, as is Prandtl's.

It is heretofore shown that Phillips' numerical implementation of lifting-line theory is analogous to Prandtl's, in the limit as the number of discrete horseshoe vortices approaches infinity. Therefore, its use is limited in similar ways as Prandtl's classic implementation. Its advantage to this work, however, lies in the fact that no integration is required in its application, in contrast to the implementation derived in Section IV.A. Thus, by applying the concepts of conditional concavity and jointed trailing vortices, a general, numerical lifting-line theory implementation is obtained.

3. Generalizations to Numerical Implementation

Recall that the local velocity at a control point is described by Eq. (71), where $\vec{v}_{ji}$ is the influence of vortex j on control point i. Using the notation in Fig. 9, and Eqs. (76) and (80), this influence can be described by the equation

$$\vec{v}_{12} = \frac{1}{4\pi}\Bigg(- \frac{\vec{u}_\infty \times \vec{r}_{a'}}{r_{a'}(r_{a'} - \vec{u}_\infty \cdot \vec{r}_{a'})} + \frac{(r_{a'} + r_a)(\vec{r}_{a'} \times \vec{r}_a)}{r_{a'} r_a (r_{a'} r_a + \vec{r}_{a'} \cdot \vec{r}_a)} + \frac{(r_a + r_b)(\vec{r}_a \times \vec{r}_b)}{r_a r_b (r_a r_b + \vec{r}_a \cdot \vec{r}_b)} + \frac{(r_b + r_{b'})(\vec{r}_b \times \vec{r}_{b'})}{r_b r_{b'} (r_b r_{b'} + \vec{r}_b \cdot \vec{r}_{b'})} + \frac{\vec{u}_\infty \times \vec{r}_{b'}}{r_{b'}(r_{b'} - \vec{u}_\infty \cdot \vec{r}_{b'})} \Bigg) \tag{85}$$

where

$$\vec{r}_a = \left[\tilde{f}_{z_2}(z_2) - \tilde{f}_{z_2}(z_a), 0, z_2 - z_a\right]$$

$$\vec{r}_{a'} = \left[\tilde{f}_{z_2}(z_2) - \tilde{f}_{z_2}(z_a) - \frac{\delta}{\sqrt{1 + \tilde{f}'_{z_2}(z_a)^2}}, 0, z_2 - z_a + \frac{\delta \tilde{f}'_{z_2}(z_a)}{\sqrt{1 + \tilde{f}'_{z_2}(z_a)^2}}\right]$$

$$\vec{r}_b = \left[\tilde{f}_{z_2}(z_2) - \tilde{f}_{z_2}(z_b), 0, z_2 - z_b\right]$$

$$\vec{r}_{b'} = \left[\tilde{f}_{z_2}(z_2) - \tilde{f}_{z_2}(z_b) - \frac{\delta}{\sqrt{1 + \tilde{f}'_{z_2}(z_b)^2}}, 0, z_2 - z_b + \frac{\delta \tilde{f}'_{z_2}(z_b)}{\sqrt{1 + \tilde{f}'_{z_2}(z_b)^2}}\right]$$

$$\vec{u}_\infty = \left[u_x, u_y, u_z\right]$$

with $\tilde{f}_{z_2}$ and $\tilde{f}'_{z_2}$ as defined in Eqs. (19)-(20) and the locus of aerodynamic centers defined using Eqs. (43)-(45). Note

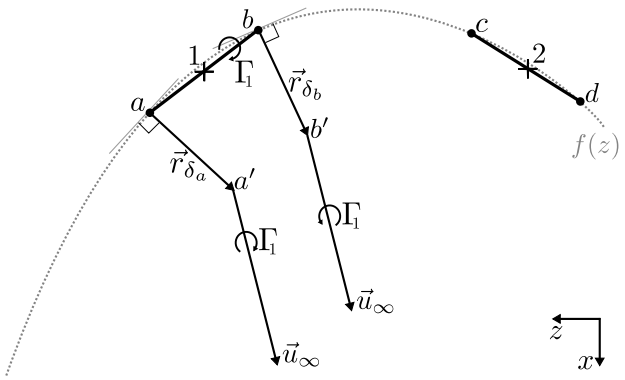

Fig. 9 The velocity induced at a point by the jointed horseshoe vortex 1, on the control point 2.

that, in the case where $i = j$, the third term on the right-hand-side of Eq. (85) (i.e. the term describing the influence of the bound vortex segment) should be omitted from the calculation, because the control point is located on the bound vortex segment itself. This should analytically result in zero induced velocity, but, in practice, round-off errors in the control point's location result in high, non-zero velocities.

Once the influence of the horseshoe vortices is calculated using Eq. (85), Eq. (74) is solved to predict the circulation at each spanwise position along the wing. This implementation of lifting-line theory can be applied to the more-general cases of wings with sweep, and wings in sideslip. This general applicability is validated in the following section, along with a study of the effects of $\Delta\tilde{z}_{98\%}$ and δ/c on the solution.

V. Examination and Validation of General, Numerical Lifting-Line Implementation

The general, numerical implementation of lifting-line theory described in Section IV.B is dependent on the joint length of the trailing vortices, δ/c, and the blending length used to calculate the effective loci of aerodynamic centers, $\Delta\tilde{z}_{98\%}$. The sensitivity of the implementation to these two parameters is examined by comparing the circulation distributions predicted, while varying $\Delta\tilde{z}_{98\%}$ and δ/c, for an increasing number of nodes along the span (between $n = 20$ and $n = 640$). The root-mean-square (RMS) change between circulation distributions as the node count doubles is calculated to determine the convergence of the results as the number of nodes increases to infinity using Richardson extrapolation [21]. For a convergent numerical algorithm, it is expected that the RMS change in the predicted circulation distribution will tend to zero as the number of nodes used in the computation increases. Furthermore, the numerical algorithm's efficiency is measured by the rate at which the RMS change approaches its fully refined value (i.e. at $n = \infty$). In addition to the examination of the RMS's convergence, the sensitivity of the implementation is examined by calculating the change in total lift coefficient, ∇C_L, as a function of δ/c and $\Delta\tilde{z}_{98\%}$. Finally, the accuracy of the general lifting-line implementation is examined through a comparison to a high-fidelity aerodynamic prediction method and experimental data.

A. Initial Observations

Preliminary results from the general, numerical lifting-line implementation show that the use of conditional concavity and jointed trailing vortices produce a convergent lifting-line theory implementation for wings with sweep and wings in sideslip. Figures. 10–11 show the total lift coefficient and the RMS change between the circulation distributions as the number of nodes along the span increases, as predicted by Phillips' implementation and the general implementation, for a wing with 45° sweep and aspect ratio of 5 with a NACA 0012, at $\alpha = \beta = 5°$. Notice that the circulations predicted by Phillips' implementation in Fig. 10 continue to change with an increasing node count, never converging to a single distribution. On the other hand, the general implementation of lifting-line in Fig. 11 predicts nearly the same circulation distribution for all node counts, demonstrating a grid-convergent solution.

Note that, in Fig. 10, the circulation distribution predicted by Phillips' implementation approaches zero at the root of the wing. Recall, from Eq. (15), that either the concavity of the locus of aerodynamic centers or the circulation must tend to zero if the influence at a control point is to remain finite. Because Phillips' implementation models the locus of aerodynamic centers as the quarter-chord line of the wing, the concavity is non-zero at the root, and the circulation is being forced to zero.

From Fig. 10 it is predicted that, with an infinite number of uniformly distributed nodes, the RMS change in the circulation distribution predicted by Phillips' implementation will be 3×10^{-3}, after converging at a rate of 0.353. Conversely, from Fig. 11 the general implementation is predicted to have an RMS change of 2×10^{-5} with an infinite number of uniformly distributed nodes, converging at a rate of 0.945. A similar comparison is observed with the convergence of the total lift coefficient. The total lift coefficient predicted by Phillips' implementation converges at a rate of 0.204, whereas the general implementation demonstrates a convergence rate of 0.927. This difference in grid-convergence demonstrates the advantage that the addition of jointed trailing vortices and conditional concavity provides to the general lifting-line implementation, as compared to Phillips' original numerical implementation.

B. Sensitivity to Joint Length

To isolate the effect of the trailing vortex joint length, δ/c, on the lifting-line results, the case of a straight, rectangular wing in sideslip will be considered. Because the locus of aerodynamic centers is a straight line for a straight, rectangular wing (see Eq.(43)) $\Delta\tilde{z}_{98\%}$ does not affect the solution in this case. Therefore, the lifting-line implementation's sensitivity to δ/c can be explored, unaffected by the locus of aerodynamic centers.

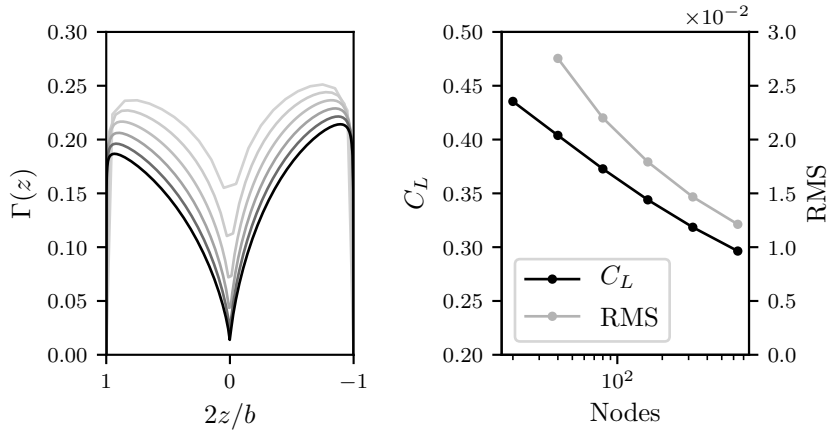

Fig. 10 The circulation distribution of a rectangular wing, with NACA 0012 airfoil sections, predicted by Phillips' implementation [11], for several node counts, dark (n_{max}) to light (n_{min}) ($\Delta\tilde{z}_{98\%} = 0.0$ and $\delta/c = 0.0$) (left). The RMS change in the circulation distributions and total lift coefficient as a function of the node count (right).

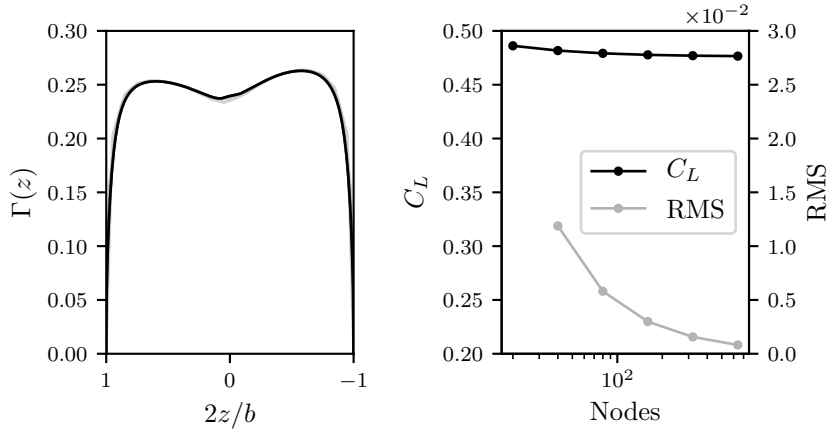

Fig. 11 The circulation distribution of a rectangular wing, with NACA 0012 airfoil sections, predicted by the general implementation, for several node counts, dark (n_{max}) to light (n_{min}) ($\Delta\tilde{z}_{98\%} = 0.25$ and $\delta/c = 0.15$) (left). The RMS change in the circulation distributions and total lift coefficient as a function of the node count (right).

Table 1 shows the parameters that are varied to study the joint-length sensitivity of the general lifting-line implementation. Each parameter is sampled at frequent intervals along its designated range, while all others are held at a "standard" value. For each case, the RMS convergence rate and extrapolated value is recorded, along with the convergence of the lift coefficient and its predicted sensitivity to δ/c. The results are shown in Figs. 12–14.

From the results show in Figs. 12–14, it can be observed that convergence and extrapolated values remain largely unaffected once δ/c is above a value of approximately 0.15. The convergence rates for both RMS and C_L demonstrate first-order convergence, the extrapolated RMS values approach values very close to zero, and the change in extrapolated lift coefficient values remain relatively constant. Additionally, above this threshold for joint length, the convergence of the implementation is independent of angle of attack and side-slip and only demonstrates slight variations with changes in aspect ratio. The first-order convergence observed in these studies is consistent with the order of the approximations made in Phillips' numerical implementation of lifting-line. The continuous trailing vortex sheet and variable-strength bound vortex are replaced by a set of constant strength horseshoe vortices, resulting in a first-order approximation of the

Table 1 Summary of Parameters Varied in Joint Sensitivity Study

Parameter	Min. Value	Max. Value	Std. Value
δ/c	0	1	—
β	0°	45°	30°
α	−5°	10°	5°
R_A	2	24	8

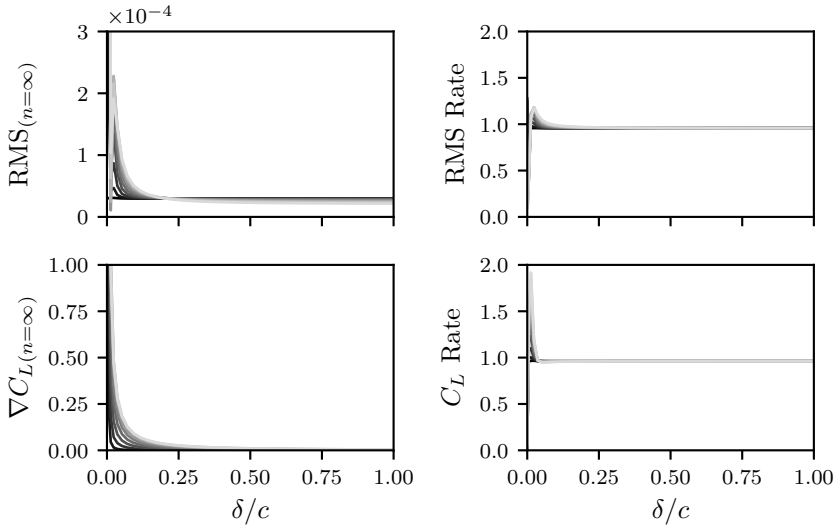

Fig. 12 The sensitivity of the general lifting-line implementation's convergence rate and results to joint length and side-slip angle, dark (β_{min}) to light (β_{max}).

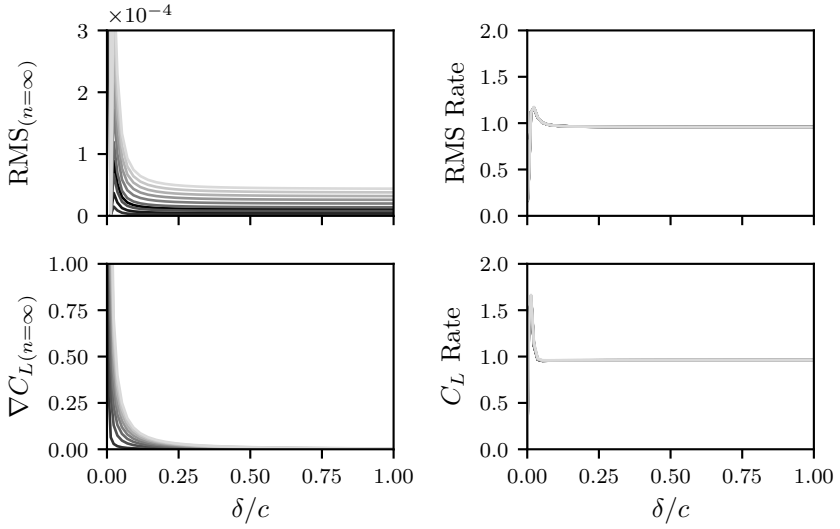

Fig. 13 The sensitivity of the general lifting-line implementation's convergence rate and results to joint length and angle of attack, dark (α_{min}) to light (α_{max}).

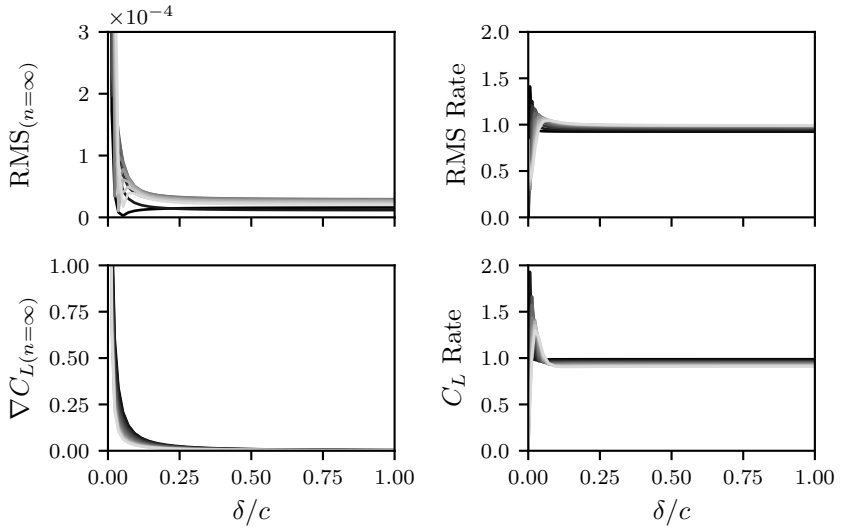

Fig. 14 The sensitivity of the general lifting-line implementation's convergence rate and results to joint length and aspect ratio, dark ($R_{A_{\min}}$) to light ($R_{A_{\max}}$).

continuous system.

Below the threshold of $\delta/c \approx 0.15$, the results produced by the general implementation of lifting-line are less desirable. The convergence of the lift coefficient and RMS become highly dependent on the joint length, and, in some cases, approach a convergence rate of zero. The lift coefficient also becomes more sensitive to changes on the joint length as δ/c approaches zero. Similarly, the extrapolated values of the RMS drastically increase at low joint lengths, replicating the non-convergence circulation distributions produced by Phillips' implementation. It is therefore apparent that a value of the joint length must be chosen such that $\delta/c \gtrsim 0.15$, to avoid these undesirable results.

C. Sensitivity to Conditional Concavity Strength

Unlike the joint length parameter, δ/c, there is not an effective means of isolating the effective locus of aerodynamic centers blending length, $\Delta\tilde{z}_{98\%}$, for observation. The locus of aerodynamic centers is modeled using Küchemann's equation from Eq. (43), resulting in non-perpendicular trailing vortices and the need for a finite joint length. Therefore, the cases of swept, rectangular wings used to test the sensitivity of $\Delta\tilde{z}_{98\%}$ will also be influenced by any effects from δ/c. Fortunately, based on the results of the previous section, the effects of joint length will be small for a large enough value of δ/c.

The parameters varied to study of the effects the blending length are shown in Table 2. Again, for each case the RMS convergence rate and extrapolated value is recorded, along with the convergence and sensitivity of the lift coefficient, and each parameter is sampled at frequent intervals along its feasible range, while all others are held at a "standard" value, see Table 2. The results are shown in Figs. 15–19, relative to blending length, $\Delta\tilde{z}_{98\%}$, as defined in Eq. (22).

Table 2 Summary of Parameters Varied in Blending Length Sensitivity Study

Parameter	Min. Value	Max. Value	Std. Value
$\Delta\tilde{z}_{98\%}$	0.01	2	—
Λ	$-30°$	$60°$	$30°$
δ/c	0.1	1	0.15
β	$0°$	$20°$	$5°$
α	$-5°$	$10°$	$5°$
R_A	2	24	8

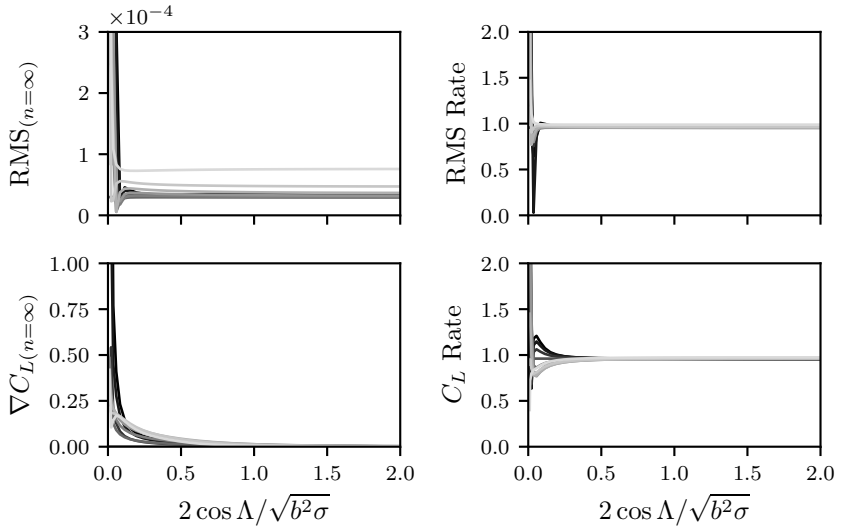

Fig. 15 The sensitivity of the implementation's convergence rate and results to blending strength and sweep, dark ($\Lambda_{\mathbf{min}}$) to light ($\Lambda_{\mathbf{max}}$).

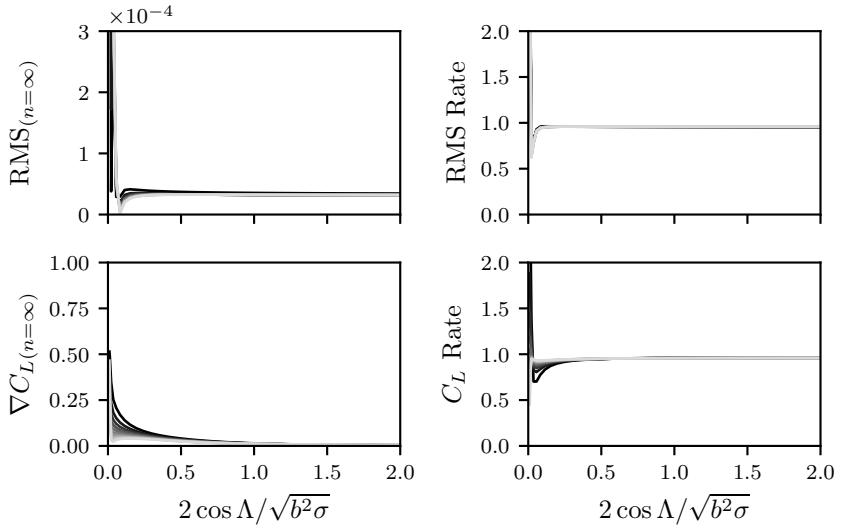

Fig. 16 The sensitivity of the implementation's convergence rate and results to blending strength and joint length, dark ($\delta_{\mathbf{min}}/c$) to light ($\delta_{\mathbf{max}}/c$).

The results in Figs. 15–19 show similar behavior as that observed in the joint-length sensitivity study. Namely, for blending lengths above a given threshold, in this case approximately 0.25, the results remain essentially unaffected. The convergence rates for both the RMS and lift coefficient again demonstrate first-order convergence, with little to no variation with respect to any of the varied parameters. The extrapolated RMS values and lift sensitivity also show little variation once the blending length is above the threshold. In contrast, as the blending length tends to zero, the convergence rates are more erratic, the extrapolated RMS values sharply increase, and the lift coefficients become more sensitive to $\Delta\tilde{z}_{98\%}$. It is therefore advisable that the blending length be chosen such that $\Delta\tilde{z}_{98\%} \gtrsim 0.25$, to ensure consistent convergence and minimal sensitivity in predicted results.

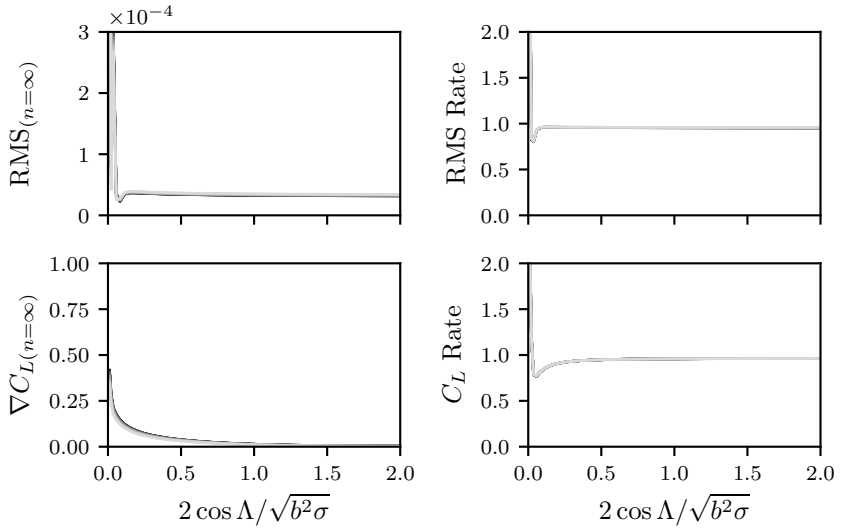

Fig. 17 The sensitivity of the implementation's convergence rate and results to blending strength and side-slip angle, dark (β_{min}) to light (β_{max}).

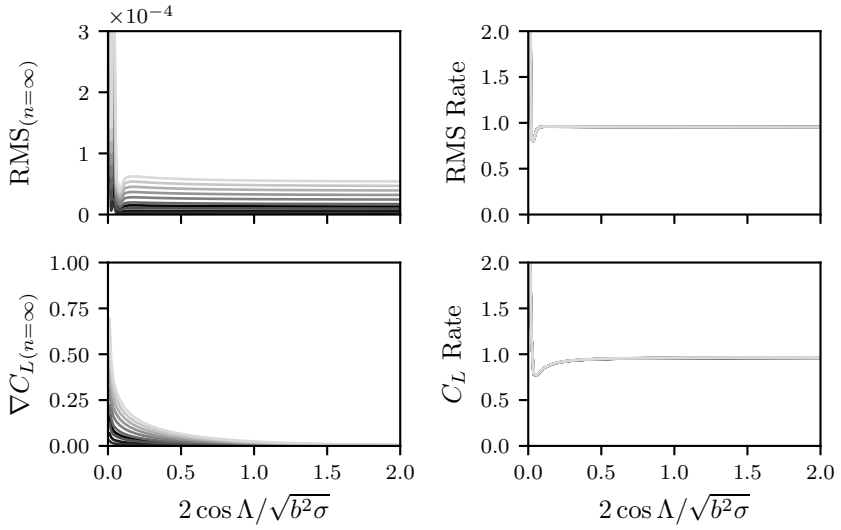

Fig. 18 The sensitivity of the implementation's convergence rate and results to blending strength and angle of attack, dark (α_{min}) to light (α_{max}).

D. Effect of Taper and Node Clustering

The cases studied to this point have only considered rectangular wings. Therefore, the effect of wing taper merits consideration. In Figs. 20 and 21, the results are shown for the "standard" wing described in Table 2, with $\Delta\tilde{z}_{98\%} = 0.25$ and taper ratios ranging from zero to one. Figure 20 shows the extrapolated values for the total lift coefficient, C_L, and the RMS change in circulation distribution as node count doubles. The solid lines in Fig. 20 are the results from the uniform node distribution used in the analytic developments and numerical cases up to this point. It is observed that the the RMS change is on the same order of magnitude as that of previous cases (0.5×10^{-4}) for the majority of taper ratios, but does exhibit a significant increase at taper ratios less than 0.1. Similarly, the curve of the lift coefficients is seen to experience two outlying points around $R_T \approx 0.1$, though it maintains a smooth, and expected behavior across the rest of

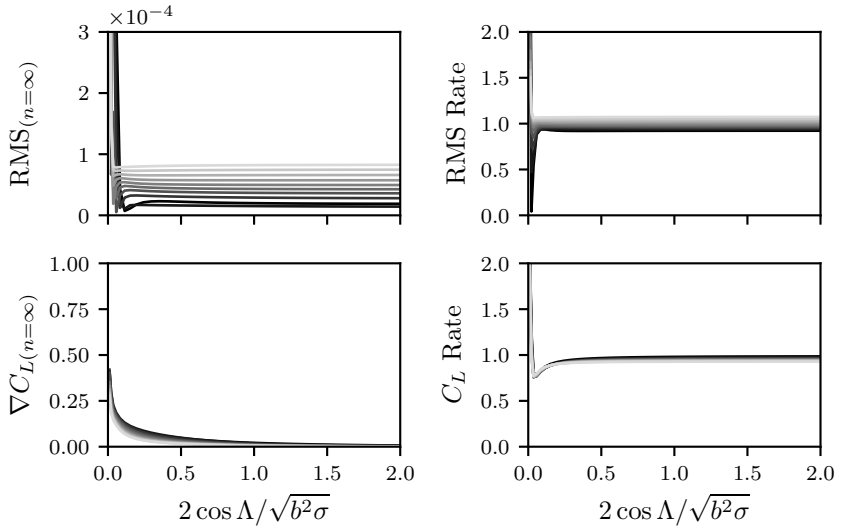

Fig. 19 The sensitivity of the implementation's convergence rate and results to blending strength and aspect ratio, dark ($R_{A_{\min}}$) to light ($R_{A_{\max}}$).

the domain.

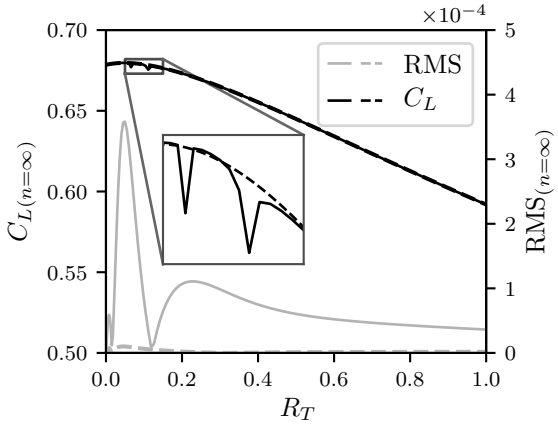

Fig. 20 The effect of taper ratio, R_T, and node clustering on the extrapolated lift coefficient and RMS change values (uniform: —; clustered: - - -).

The behavior observed in Fig. 20 at low taper ratios is corroborated and explained by the information contained in Fig. 21. The convergence of the lift coefficient and RMS (again represented as solid lines for the uniform node distribution) are consistent around one for most taper ratios, but exhibit erratic behavior below a taper ratio of 0.2. The convergence of the lift coefficient drops almost to zero twice around $R_T \approx 0.1$, explaining the outliers observed in Fig. 20. Similarly, the dip in the convergence of the RMS around 0.05 is likely the cause of the spike in RMS extrapolated value.

It is common in numerical algorithms to cluster the nodes in areas that have high gradients to improve the convergence and accuracy of the results. Lift distributions over finite wings experience the highest gradients at the tips, and swept wings can also experience higher gradients at the root. Therefore, as a comparison to a uniform node distribution, consider the *cosine clustering* of the nodes and control points at the root and tip of the wing, such that the spacing between nodes is less at the root and tip, and greater along the mid-span of the wing, as suggested by Phillips [11]. The dashed lines in Figs. 20 and 21 display the effect that this clustering has on the results for the tapered wings.

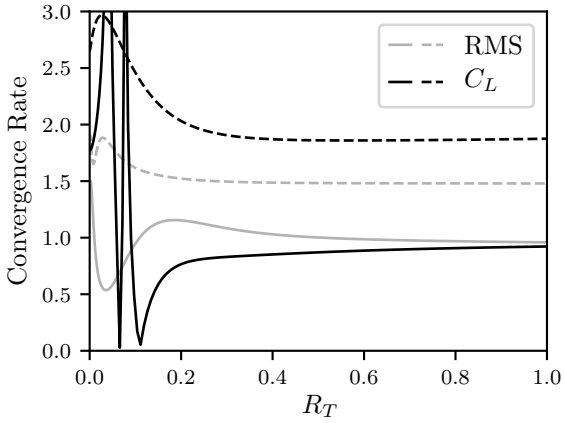

Fig. 21 The effect of taper ratio, R_T, and node clustering on the lift coefficient and RMS change convergence rates (uniform: —; clustered: - - -).

In Fig. 20, the results produced using the clustered nodes are seen to be without the defects resulting from the uniform distribution. The extrapolated lift coefficient values obtained from both distributions lay on top of one another, save for around $R_T \approx 0.1$, where the results of the clustered distribution do not include the spikes seen in the results of the uniform distribution results. The RMS values are also seen to improve when using the clustered node spacing, resulting in RMS values at least an order of magnitude less than those resulting from the uniform node distribution. Furthermore, in Fig. 21, the convergence rates for both the RMS and lift coefficient benefited from the node clustering. The lift coefficient demonstrates second-order convergence with the clustered nodes, and the RMS shows a convergence rate of about 1.5. The higher convergence rates extend to the lower taper ratios as well, eliminating the erratic behavior observed when using the uniform node distribution.

E. Accuracy of the General, Numerical Lifting-Line Implementation

Having considered the sensitivity of the general implementation to blending and joint length, its accuracy in predicting the aerodynamic properties of physical wings is studied. Consider the rectangular wing with 45° sweep and a symmetric airfoil with 12% thickness, for which experimental results are readily available from Weber and Brebner [22]. For this case, predictions are obtained using the general lifting-line implementation, Phillips' lifting-line implementation [11], and PAN AIR, a high-order panel method [23]. The predictions are compared against Weber's experimental results in Figs. 22–24. The results obtained from PAN AIR were generated using a mesh sufficiently resolved in both the chordwise and spanwise directions. Both implementations of lifting-line used 121 clustered nodes, and the effective airfoil properties of a NACA 0012 at the respective effective sweep angles. Additionally, the joint length and blending length of the general implementation were set to the standard values used in the previous studies, respectively 0.15 and 0.25. No viscous corrections were used in any of the numerical methods, and to maintain consistency with the other inviscid methods, the endcaps of the PAN AIR simulations were truncated in the results.

Figure 22 displays the section lift distributions predicted by each method, normalized by the total lift coefficient. The bars on the normalized experimental data in Fig. 22 represent the spread of the data due to viscous effects. It is seen in Fig. 22 that both the general lifting-line implementation and PAN AIR predict distributions similar in shape to the experimental results. The lift distribution predicted by Phillips' implementation, on the other hand, does not replicate the shape of the experimental distribution, drastically underpredicting the lift at the center and overpredicting the lift at the tip.

The total wing lift coefficients predicted by the four methods are shown in Fig. 23, as functions of the section lift coefficient of an infinite wing with the same airfoil, C_{L_∞}. The values of C_{L_∞} for the three inviscid numerical prediction methods were found using a 2-D vortex panel method, resulting in a 2-D section lift slope of 6.907. Though Weber doesn't report the 2-D lift slope of the airfoil used in his work, experimental results from other sources predict a viscous lift slope of 5.935 [24]. Again, general lifting-line and PAN AIR do a good job replicating the results of the experimental work, whereas Phillips' method is further removed. Recall, from Fig. 10, that Phillips' lifting-line implementation

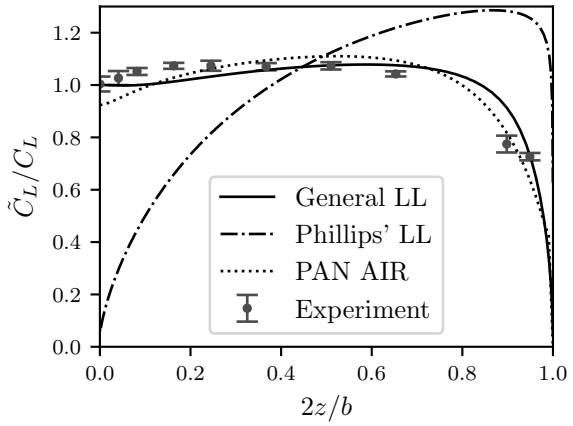

Fig. 22 A comparison of the lift distribution, as predicted by the general lifting-line implementation, Phillips' implementation [11], the panel method PAN AIR [23], and experimental data by Weber and Brebner [22].

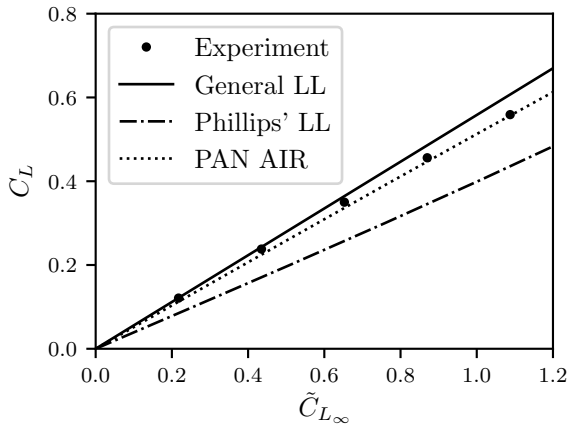

Fig. 23 A comparison of the total lift coefficient, as predicted by the general lifting-line implementation, Phillips' implementation [11], the panel method PAN AIR [23], and experimental data by Weber and Brebner [22].

for swept wings is highly dependent on the number of nodes used in the computation, and the results shown here are fixed to the number of nodes used in the general lifting-line computations. It is therefore conceivable that Phillips' implementation will yield different results if the node count is changed. General lifting-line shows better agreement with the experimental results at lower lift coefficients, where the effects of viscosity are the least. PAN AIR does a better job matching the lift coefficients of the experiments at high lift coefficients, most likely due to the fact it explicitly calculates chordwise effects of the flow.

The drag predicted by the various methods is compared in Fig. 24. The numerical methods, being inviscid, predict only induced drag, whereas the experimental results are subject to viscous effects that increase the drag, such as chordwise and spanwise boundary layer growth. Therefore, it is expected that an inviscid numerical method under-predicts the drag. Both the general implementation of lifting-line and PAN AIR conform to this expectation. The under-prediction is small at low lift coefficients and increases with increasing lift, where the effects of viscosity are increasingly dominant. On the other hand, there is an over-prediction of drag by Phillips' implementation of lifting-tine theory. The high drag prediction by Phillips's method is likely because the implementation predicts a circulation distribution with high gradients, $d\Gamma/dz$, along the majority of the wing, increasing the induced drag by increasing the overall strength of the trailing vortex sheet.

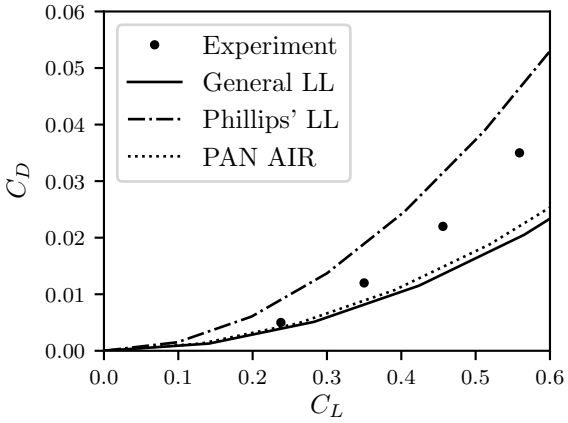

Fig. 24 A comparison of the total drag coefficient, as predicted by the general lifting-line implementation, Phillips' implementation [11], the panel method PAN AIR [23], and experimental data by Weber and Brebner [22].

The comparisons between the general lifting-line implementation, Phillips' lifting-line implementation, PAN AIR, and Weber's experimental results serve to validate the accuracy of general lifting-line implementation. The lift distribution, total lift coefficients, and total drag coefficients predicted by general lifting-line show agreement with those of PAN AIR and the experimental results and show the rectification of the issues faced when applying Phillips' method to wings with sweep. It is also worth noting that the close corroboration by the general lifting-line implementation is attained at a computational cost of fractions of a second for each minute required by PAN AIR.

VI. Conclusion

Lifting-line theory maintains that the flow over a finite, high-aspect-ratio wing is sufficiently represented by a sheet of semi-infinite vortices extending from a variable strength vortex filament placed along the locus of aerodynamic centers of the wing. Prandtl's classical implementation of lifting-line theory has been in wide use, and provides valuable intuition into the aerodynamic behavior of finite wings. However, lifting-line theory in Prandtl's classical form is restricted to straight wings in flows without sideslip. Similarly, the numerical implementation of lifting-line theory, developed by Phillips, suffers from an inability to grid-converge for any case other than the wings covered by the classical implementation of the theory, though it removes the need for integration in the calculation of induced velocities. It is therefore necessary to consider the reasons for the limitations of these two implementations of lifting-line theory, before constructing a more-general implementation.

The principle limiter on the previous lifting-line theory implementations is the model of induced velocities. In order for the total velocity induced by the vortex filament, at a point along its length, to remain finite, the second derivative of the vortex filament, which lies along the locus of aerodynamic centers, must be zero, and the trailing vortices must be perpendicular to the locus, in the neighborhood of the point of interest. Thus, the second derivative of the locus of aerodynamic centers is forced to zero at the point and blended with the original curve for minimal impact at the other points along the wing's span. The result is an effective locus of aerodynamic centers for each point along the bound vortex filament. Furthermore, each trailing vortex is jointed, such that there is a finite segment of the trailing vortex perpendicular to the locus of aerodynamic centers and a semi-infinite portion aligned with the freestream. The modifications to the bound vortex filament and trailing vortex sheet provide the flexibility needed to implement lifting-line theory for wings with sweep or in sideslip. In addition to the considerations given to the evaluation of the induced velocity, consideration is given to modeling the locus of aerodynamic centers of non-straight wings and the section aerodynamic properties of such wings.

Following Prandtl's classical methodology, but allowing for generalizations of freestream direction and wing geometry, an analytic implementation is formed, but is too mathematically complex to be effectively applied. Thus, the general implementation of lifting-line theory is based in Phillips' numerical algorithm. The resulting application

of lifting-line theory is able to predict the circulation distribution of wings with sweep in sideslip, with numerical convergence. The study of the sensitivity of the general lifting-line implementation to the blending and joint lengths demonstrates that the convergence of the method is insensitive to these parameters, so long as they remain above the requisite threshold (i.e. $\delta/c \gtrsim 0.15$ and $\Delta\tilde{z}_{98\%} \gtrsim 0.25$). Furthermore, this implementation of lifting-line theory is shown to be accurate when compared to experimental results, and results from a higher-fidelity panel method.

The results in Section V.E were obtained using largely arbitrary values for δ/c and $\Delta\tilde{z}_{98\%}$, with the purpose of demonstrating the "out of the box" capability of the general implementation. In practice, these values could be tuned, to further improve the agreement between the general lifting-line implementation and a specific case-study. However, the sensitivity studies performed herein suggest that such tuning would only provide relatively small variations in the calculated results. Rather, a more effective method of tuning the accuracy of the general implementation may be through modification of the airfoil section properties used in the computation.

The implementation of lifting-line theory derived herein may be deemed a "general" formulation because, while Phillip's implementation is indeed a "modern" approach to Prandtl's lifting-line, in the sense that it takes advantage of modern computing power, it does not, in effect, expand upon Prandtl's implementation (save for the ability to analyze multiple straight wings, with zero sideslip). The method derived in this work is shown to be applicable and convergent for a wide range of swept and tapered wings, in a wide variety of flow conditions.

Acknowledgments

The author would like to thank the Utah State University Office of Research and Graduate Studies and Mechanical and Aerospace Engineering Department for funding this work through the Presidential Doctoral Research Fellowship (PDRF) program. Additional funding for this work was provided by the U.S. Office of Naval Research Sea-Based Aviation program (Grant No. N00014-18-1-2502) with Brian Holm-Hansen as the program officer.

References

[1] Anderson, J. D., *Fundamentals of Aerodynamics*, 5th ed., McGraw-Hill, 2011, Chaps. 4-5, pp. 361–67, 411–457.

[2] Kuchemann, D., *The Aerodynamic Design of Aircraft*, 1st ed., Pergamon Press Ltd, 1978.

[3] Phillips, W. F., *Mechanics of Flight*, 2nd ed., John Wiley & Sons, Inc., 2010, Chap. 1, pp. 32–107.

[4] Karamcheti, K., *Principles of Ideal-Fluid Aerodynamics*, Wiley, 1966, Chap. 19, pp. 548–554.

[5] Weissinger, J., "The Lift Distribution of Swept-Back Wings," Tech. rep., National Advisory Commitee for Aeronautics, 1947.

[6] Barnes, J. P., "Semi-Empirical Vortex Step Method for the Lift and Induced Drag Loading of 2D or 3D Wings," *World Aviation Conference*, 1997.

[7] Rosen, A., and Rand, O., "The Aerodynamics Behavior of Infinite Swept Wing: Another Point of View," *Journal of Aircraft*, Vol. 22, No. 1, 1985, pp. 83–85.

[8] Ashenberg, J., "Curved lifting-line theory for thin planar wings," *Israel Journal of Technology*, Vol. 20, 1982.

[9] Beyer, F., Matha, D., Sebastian, T., and Lackner, M., "Development, Validation and Application of a Curved Vortex Filament Model for Free Vortex Wake Analysis of Floating Offshore Wind Turbines," *50th AIAA Aerospace Sciences Meeting including the New Horizons Forum and Aerospace Exposition*, 2012, p. 371.

[10] Bliss, D. B., Teske, M. E., and Quackenbush, T. R., "A new methodology for free wake analysis using curved vortex elements," 1987.

[11] Phillips, W. F., and Snyder, D. O., "Modern Adaptation of Prandtl's Classic Lifting-Line Theory," *Journal of Aircraft*, Vol. 37, No. 4, 2000, pp. 662–670.

[12] Helmbold, H., "Der unverwundene ellipsenflugel als tragende flanche," *Jahrbuch*, 1942, pp. I111–I113.

[13] Snyder, D., and Memory, C., "A Modified Vortex Algorithm for Low Reynolds Number, Low Aspect-Ratio Wings," *23rd AIAA Applied Aerodynamics Conference*, 2005, p. 4608.

[14] James Ward Brown, R. V. C., *Complex Variables and Applications*, 8th ed., McGraw-Hill, 2009, Chap. 7.

[15] Kreysig, E., *Advanced Engineering Mathematics*, 8th ed., Wiley, 1999, Chap. 15, pp. 787–793.

[16] Hunsaker, D., and Phillips, W. F., "A Numerical Lifting-Line Method Using Horseshoe Vortex Sheets," *Utah Space Grant Consortium*, 2011.

[17] Kuchemann, D., "A Simple Method for Calculating the Span and Chordwise Loading on Straight and Swept Wings of any Given Aspect Ratio at Subsonic Speeds," Tech. rep., Aeronautical Research Council, 1956.

[18] Moorthamers, B., and Hunsaker, D. F., "Accuracy of Küchemann's Prediction for the Locus of Aerodynamic Centers on Swept Wings," *AIAA SciTech*, 2020.

[19] Reid, J. T., and Hunsaker, D. F., "Effect of Sweep on Airfoil Section Properties," *AIAA SciTech Forum*, 2019, p. 2118.

[20] Acton, F., *Numerical Methods that Work*, MAA spectrum, Mathematical Association of America, 1990, Chap. 15. URL `https://books.google.com/books?id=cGnSMGSE5Y4C`.

[21] Celik, I. B., "Journal of Fluids Engineering Editorial Policy Statement on the Control of Numerical Accuracy," 2000.

[22] Weber, J., and Brebner, G., "Low-Speed Tests on 45-deg Swept-Back Wings, Part I," Technical Report 2882, Aeronautical Research Council Reports and Memoranda, 1958.

[23] Magnus, A. E., and Epton, M. A., "PAN AIR: A computer program for predicting subsonic or supersonic linear potential flows about arbitrary configurations using a higher order panel method. Volume 1: Theory document (version 1.1)," 1981.

[24] McCroskey, W., "A critical assessment of wind tunnel results for the NACA 0012 airfoil," Tech. rep., NASA Ames, Moffett Field, CA, 1987.